



Chem Soc Rev

**Polymers under nanoconfinement: Where are we now in understanding local property changes?**

Journal:	<i>Chemical Society Reviews</i>
Manuscript ID	CS-REV-01-2021-000054.R1
Article Type:	Review Article
Date Submitted by the Author:	22-Apr-2021
Complete List of Authors:	Roth, Connie; Emory University, Department of Physics

SCHOLARONE™  
Manuscripts

# Polymers under nanoconfinement: Where are we now in understanding local property changes?

Connie B. Roth\*

Submitted to *Chemical Society Reviews*: January 15, 2021; Revised version submitted: April 22, 2021

Polymers are increasingly being used in applications with nanostructured morphologies where almost all polymer molecules are within a few tens to hundreds of nanometers from some interface. From nearly three decades of study on polymers in simplified nanoconfined systems such as thin films, we have come to understand property changes in these systems as arising from interfacial effects where local dynamical perturbations are propagated deeper into the material. This review provides a summary of local glass transition temperature  $T_g$  changes near interfaces, comparing across different types of interfaces: free surface, substrate, liquid, and polymer-polymer. Local versus film-average properties in thin films are discussed, making connections to other related property changes, while highlighting several historically important studies. By experimental necessity, most studies are on high enough molecule weight chains to be well entangled, although aspects that connect to lower molecule weight materials are described. Emphasis is made to identify observations and open questions that have yet to be fully understood such as the evidence of long-ranged interfacial effects, finite domain size, interfacial breadth, and chain connectivity.

## 1 Introduction

In the field of polymers, “nanoconfinement” has come to refer to system sizes and sample geometries where the polymer material is confined to some small size — whether this be film thickness, layer thickness, domain size, etc. — for which the properties of the polymer material become perturbed from their bulk values. Typically this occurs at size scales within the nanometer range, hence the term “nanoconfinement”. Deviations from bulk properties are usually observed for size scales of a few to tens of nanometers, although effects have also been observed for many tens to hundreds of nanometers. Thus, nanoscale dimension can broadly refer to any size scale less than a micron depending on the effects being observed. Because the underlying cause for many of these property changes with system size appears to be predominantly caused by interfacial effects when surface-to-volume ratios become large, nanoconfinement has also more broadly come to refer to polymer materials that are within close proximity to a perturbing interface — again within some small nanoscale dimension where properties are expected to be perturbed. Thus, polymers under nanoconfinement can also refer to macroscopic systems with nanometer-sized filler, i.e., polymer nanocomposites, or multi-component polymer materials with numerous interfaces between small nanometer sized domains such as nanostructured polymer blends.

From a materials design perspective, there is great interest in understanding how the properties of polymers change at small size scales or near interfaces as many advanced applications re-

quire multicomponent systems with nanostructured morphologies. For polymer blends, it has long been known that smaller domain sizes lead to better material performance,<sup>1</sup> resulting in the pursuit of nanostructured polymer blends.<sup>2</sup> Historically, it was quite common during analysis to simply assume that each domain still had properties equivalent to its bulk counterpart after being blended. We have now come to appreciate that this is likely not true. Thus, there is great interest in understanding how the properties of these domains are perturbed as the resulting material performance and global properties reflect an amalgam of all its local property changes.

One can envision a future scenario where enough is known about how local properties change near different kinds of interfaces that the desired global properties of the material can be designed computationally from the ground up, perhaps with the help of machine learning, to give an optimized morphology that will result in the correct combination of local property changes for the chosen application. Such strategic use of interfacial interactions could ideally lead to a new class of high performance multicomponent materials where the desired properties are engineered right from the local nanoscale level.

The focus of the present review is to summarize where we are now with our understanding of local property changes near interfaces and to identify open questions that still need addressing to move us toward to this grand goal. The emphasis here is on a phenomenological description of the available experimental results and how they provide a picture of what factors are important to the behavior of nanoconfined systems. The glass transition temperature  $T_g$ , specifying the temperature at which the material transitions from an equilibrium liquid to a nonequilibrium glass,

*Department of Physics, Emory University, Atlanta, Georgia 30322, USA. E-mail: cbroth@emory.edu*

is the most heavily studied property, and thus provides the basis of our foundation, with its connection to other related material properties also discussed. A full theoretical understanding of the underlying physics that is responsible for the observed behavior in nanoconfined systems is still limited by the lack of an accepted theoretical description of the glass transition in bulk. However, the behavior of glasses in thin films and near interfaces has frequently served as a test-bed for such theoretical models. A comprehensive summary of the current state of the various theoretical approaches in nanoconfined films was recently provided by Schweizer and Simmons, and the reader is referred there for a detailed analysis.<sup>3</sup>

## 2 Local vs. Average Film Properties

Polymer thin films, which have a geometry with confinement in only one dimension, provide a simplified system where interfacial interactions can be interrogated in a controlled manner as a function of decreasing film thickness. In such systems, one only has to contend with one or two interfacial effects depending on the specific boundary conditions of the sample geometry. For example, a “free surface” (polymer–air interface) tends to facilitate local mobility leading to a strong increase in local dynamics, while the impact of a polymer–substrate interface will depend on the given chemical interactions possible between the polymer in question and the specific substrate chemistry. The challenge with experimental measurements in thin films is the need to get sufficient measurement signal out of very small sample sizes. Frequently this is done by measuring a comparatively wide lateral dimension, averaging over a sufficiently large area of the film (millimeters), to account for the small film thickness (nanometers).

Numerous measurements of average film properties have shown deviations from bulk properties with decreasing film thickness.<sup>3–10</sup> The most heavily studied property is the glass transition temperature  $T_g$ , with various experimental techniques reporting shifts in  $T_g$  of several or even tens of Kelvin. The first of these reports in 1994, by Keddie, Jones, and Cory showed decreases in the average film  $T_g(h)$  with decreasing film thickness  $h$  for thin polystyrene (PS) films supported on silicon substrates with native oxide layers, reaching  $T_g$  reductions of  $\approx 20$  K below the bulk value ( $T_g^{\text{bulk}} \approx 100$  °C for PS) for film thicknesses  $h \approx 15$  nm.<sup>11</sup> Already during this first study it was hypothesized that the source of this  $T_g$  decrease might come from the presence of the free surface imparting a “region of enhanced mobility” to the film.<sup>11</sup> This conjecture was supported by the observation that the  $T_g(h)$  data could be fit well by a function of the form:

$$T_g(h) = T_g^{\text{bulk}} \left[ 1 - \left( \frac{\alpha}{h} \right)^\delta \right]. \quad (1)$$

The rationale for this function was the idea that the free surface might cause a near-surface mobile layer of thickness  $\xi$  whose size would diverge at  $T_g^{\text{bulk}}$  following a typical power law behavior

$$\xi(T) = \alpha \left( 1 - \frac{T}{T_g^{\text{bulk}}} \right)^{-1/\delta} \quad (2)$$

described by parameters  $\alpha$  and  $\delta$ .<sup>11</sup> The  $T_g(h)$  of the film with

a finite thickness  $h$  would then occur when the thickness of this mobile layer  $\xi(T)$  grew to encompass the entire thickness of the film, i.e.,  $\xi(T) = h$ , resulting in Eq. 1.

Also supporting this hypothesis were measurements of the average  $T_g(h)$  of free-standing PS films with two free surfaces, top and bottom, which showed even larger  $T_g$  reductions.<sup>4,12–14</sup> For a range of molecular weights  $M_w < 350$  kg/mol, the  $T_g(h)$  decrease for a free-standing film of a given thickness  $h$  was found to be twice the  $T_g(h)$  decrease for a supported film with only a single free surface.<sup>13</sup> Higher molecular weight free-standing PS films showed a more complex behavior with a strongly molecular weight dependent, linear  $T_g(h)$  decrease.<sup>4,14</sup> However, this molecular weight dependent transition has since been identified as the weaker transition, with a more dominant transition independent of molecular weight comprising  $\approx 80$ – $90$  % of the film consistent with the  $M_w < 350$  kg/mol free-standing results showing a  $T_g(h)$  decrease following Eq. 1.<sup>15,16</sup>

It was not until a decade after this initial hypothesis was proposed that two different studies reported confirmation that the free surface was in fact the source of the  $T_g$  reduction. In 2003, Sharp and Forrest showed that if the free surface was properly capped, a PS film sandwiched between two neutral substrate interfaces, showed no  $T_g(h)$  shift down to  $h = 7$  nm.<sup>17</sup> As shown by their data replotted in Figure 1, when supported PS films were capped by gold and aluminum, the  $T_g(h)$  decrease was eliminated, and when the aluminum cap was removed, the  $T_g(h)$  decrease was recovered in agreement with PS films that were uncapped. Particularly interesting was the observation that while the evaporation of a thin layer of gold atop the PS film was sufficient to cap the surface and remove the free surface effect, simply evaporating an aluminum layer in a similar manner did not remove

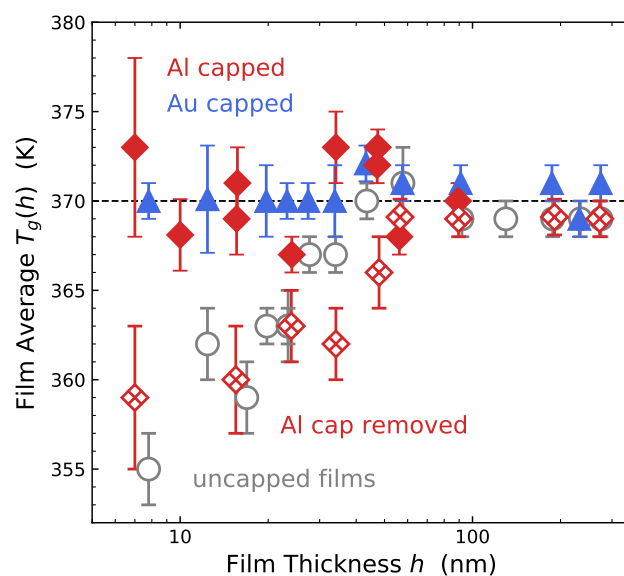


**Fig. 1** Film average glass transition temperature  $T_g(h)$  for PS films: gold capped films (blue solid triangles), aluminum capped  $2(h/2)$  films (red solid diamonds),  $2(h/2)$  films with aluminum cap removed (red  $\times$ -diamonds), uncapped films (gray open circles). [Data from Sharp and Forrest, Ref. 17.]

the PS free surface because delamination occurred between the aluminum cap and PS free surface.<sup>17,18</sup> This reduced adhesive energy between aluminum and PS, still leaving a free surface when an aluminum layer is evaporated on top of a film, has important implications for dielectric measurements where samples are routinely made in this manner. Instead, for the aluminum capped data shown in Fig. 1, the authors created two half films each of thickness  $h/2$  that were annealed together to form a single aluminum capped film of thickness  $h$ . These  $2(h/2)$  aluminum capped films did not exhibit any  $T_g(h)$  decrease with decreasing film thickness down to 7 nm, but were then also shown to recover a  $T_g(h)$  decrease when the aluminum cap was removed.<sup>17</sup>

Also reported in 2003, were results by Ellison and Torkelson using a newly developed localized fluorescence method that could measure the local  $T_g$  at different positions within a film by placing a thin layer of PS that was lightly labeled with pyrene at specific locations within the sample.<sup>19</sup> Early control measurements verified that the same film-average  $T_g(h)$  results were obtained using both free pyrene dye in the film as when the pyrene dye was covalently bonded to the polymer chains, and agreed with other experimental measures of  $T_g$  such as ellipsometry and differential scanning calorimetry (DSC) for bulk films.<sup>20–22</sup> In the 2003 study, they demonstrated that the local  $T_g$  of a 14-nm thick pyrene-labeled probe layer placed as a free-surface layer at the top of the film was reduced by 32 K from the bulk value  $T_g^{\text{bulk}}$  for PS films with total thicknesses  $h \geq 60$  nm, while an equivalent probe layer placed at the substrate interface reported  $T_g^{\text{bulk}}$ . The text of their paper also described additional measurements where the 14-nm thick pyrene-labeled probe layer was capped with different layer thicknesses of neat (unlabeled) PS providing data of how the local  $T_g$  recovered its bulk value  $T_g^{\text{bulk}}$  deeper into

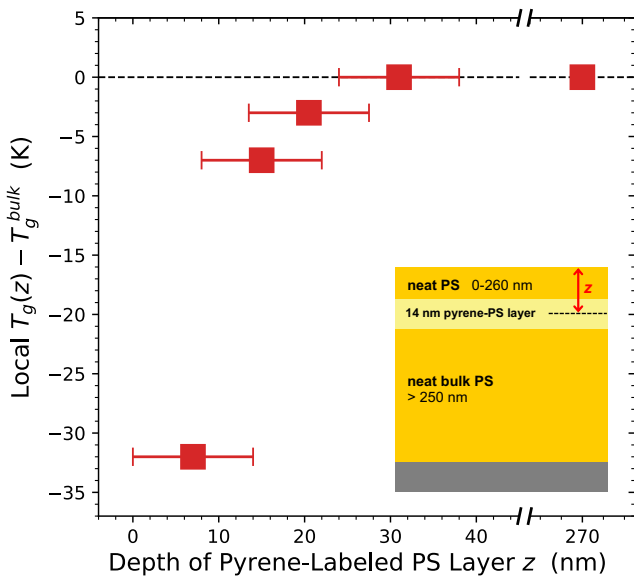


**Fig. 2** Local glass transition temperature  $T_g(z) - T_g^{\text{bulk}}$  for 14-nm thick pyrene-labeled PS layers placed at different depths from the free surface within thick PS films. Position  $z$  was set as the midpoint of the labeled layer with error bars indicating the width of the 14 nm layer. [Data from Ellison and Torkelson, Ref. 19.]

the film.<sup>19</sup> Figure 2 graphs these results providing a measure of the local  $T_g(z)$  profile next to the free surface of a bulk PS film. The samples were described as having the 14-nm pyrene-labeled probe layer placed atop a bulk PS film ( $\gtrsim 250$  nm) with an additional neat PS capping layer added of varying thickness. To graph these data in Fig. 2, the  $z$  value was chosen to be the distance from the free surface to the midpoint of the 14-nm probe layer with horizontal error bars added to illustrate the width of the probe layer. These results from Ellison and Torkelson show that the local  $T_g$  decrease occurring near the free surface continues quite deep into the film, only recovering  $T_g^{\text{bulk}}$  at a depth of  $\approx 30$  nm.

Thus, we have come to understand  $T_g(h)$  changes in thin films as resulting from a perturbation to the dynamics at the interface that is then propagated deeper into the film. Other polymers show similar behavior, however the magnitude of the perturbation caused by the free surface does depend on polymer chemistry. For example, poly(methyl methacrylate) (PMMA) exhibits a free surface effect that is approximately three times weaker than PS.<sup>23–25</sup> The impact of the substrate is also highly dependent on polymer chemistry where attractive interactions like hydrogen bonding can lead to local  $T_g$  increases,<sup>26,27</sup> which are then observed to propagate upward into the film.<sup>28</sup> An example of this would be PMMA next to a silica substrate interface, such that these supported PMMA thin films show competing interface effects with a local  $T_g$  increase (+10 K) from the silica substrate interface competing with a local  $T_g$  decrease (-7 K) from the free surface often resulting in an average film  $T_g(h)$  that is little perturbed from bulk.<sup>26,29</sup> Figure 3 provides a cartoon illustration of the local  $T_g$  values measured for thin fluorescent probe layers placed at either the free surface or substrate interface for PMMA and PS films based on work from the Torkelson group.<sup>19,26</sup>

What mechanism controls how these interfacial perturbations to dynamics propagate deeper into the film is still not clear, but we do have quite a bit of experimental data that provides insight into which factors are important. In general, the  $T_g(h)$  behavior has been shown to be independent of molecular weight for supported films.<sup>11,20,30,31</sup> Despite the film thickness at which  $T_g(h)$  starts deviating from bulk,  $\approx 60$  nm for PS, being comparable to polymer chain sizes in general, the exact same  $T_g(h)$  behavior,

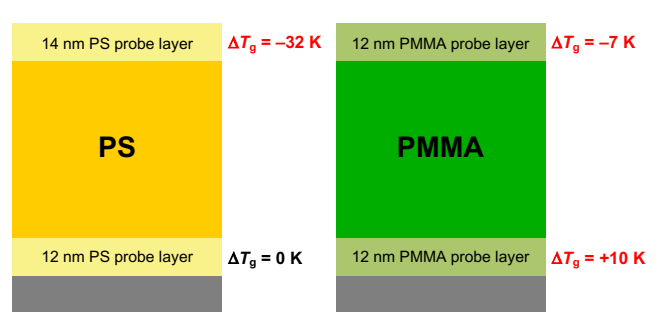


**Fig. 3** Cartoon illustrating local glass transition temperature  $\Delta T_g = T_g - T_g^{\text{bulk}}$  values for fluorescent probe layers placed at either the free surface or substrate interface of PS and PMMA bulk films (total thickness  $>250$  nm) supported on silica substrates. [Data from Torkelson et al., Refs. 19,26.]

deviating at  $\approx 60$  nm, is observed for small oligomeric molecular weights  $\sim 2$  kg/mol,<sup>20,32,33</sup> where the radius of gyration of the polymer  $R_g \approx 1$  nm, as very high molecular weights  $\sim 7000$  kg/mol where  $R_g \approx 75$  nm.<sup>31</sup> Thus, this phenomenon of accelerated interfacial dynamics is not a uniquely polymer related behavior. Most of the available experimental data exists for polymers primarily because of the ease of such measurements, whereas the viscosity of small molecule glass formers is comparatively much lower such that dewetting of the film quickly occurs.<sup>33,34</sup>

These early observations that  $T_g(h)$  changes are generally independent of chain length has led the field to treat interfacial perturbations as primarily an enthalpic effect, although efforts to correlate  $T_g(h)$  shifts with interfacial energy have not found a simple correlation.<sup>35,36</sup> Recent studies have begun reporting variations in confinement behavior for polymers with different chain architectures that otherwise have identical chemical compositions. These differences between cyclic and linear chains<sup>37–39</sup> or star polymers<sup>40–49</sup> suggest that the interface can also be a boundary that alters the available entropic conformations of polymers to a sufficient degree that their local dynamics can be perturbed. Recent studies have also reported previously unobserved molecular weight dependencies to  $T_g(h)$  changes,<sup>50–54</sup> as well as surface dynamics,<sup>55–60</sup> demonstrating that our historical interpretation of a primarily molecular weight independent phenomenon may need revision, where entropic and chain connectivity considerations may also be altering the gradient in dynamics near interfaces.<sup>31</sup>

The strength and length scale of the  $T_g(h)$  behavior have been found to vary with factors that affect molecular packing such as chain stiffness or the size and steric flexibility of side groups.<sup>20,61–63</sup> Computer simulations modeling confined polymer films have also observed variations in glass transition behavior altered by chain stiffness<sup>64,65</sup> and factors that correlate with cooperative motion.<sup>66,67</sup> Comparing a number of different polymers, Evans and Torkelson<sup>68</sup> have observed an interesting correlation between a polymer's  $T_g(h)$  behavior and its fragility,

$$m = \left. \frac{d \log \tau_\alpha}{d(T/T_g)} \right|_{T=T_g} \quad (3)$$

As fragility  $m$  characterizes the temperature-dependent change in the  $\alpha$ -relaxation time  $\tau_\alpha$  at  $T_g$ , a measure of a glass formers' speed of dynamical arrest due to packing frustrations, this correlation with  $T_g(h)$  also ties this interface phenomenon to molecular packing and glass forming ability. However efforts by Simmons et al. to find a broad correlation with fragility over a wide range of simulated glass formers have shown only weak to modest correlations.<sup>69</sup> Thus, the exact factors that determine the strength and extent of interfacial perturbations are still not known. Most theoretical efforts that aim to capture how interfacial effects alter the glass transition and other associated phenomenon treat the interface as perturbing some factor that affects cooperative motion such as a change in local energy barrier, number of cooperative units moving collectively, amount of local free volume affecting molecular mobility, etc.<sup>3</sup>

It is the glass transition and other glassy phenomena like physi-

cal aging that appear to be particularly sensitive to interfacial perturbations, perhaps because small perturbations to local mobility and packing can have such a large impact on dynamics. However, other material properties have also shown changes with decreasing film thickness. Viscous flow in thin films is accelerated, where the Vogel-Fulcher-Tammann (VFT) temperature dependence for the viscosity,

$$\eta(T) = \eta_0 \exp\left(\frac{B}{T - T_0}\right), \quad (4)$$

has the Vogel temperature  $T_0 \simeq T_g - 50$  K effectively shifted by approximately the same amount as  $T_g$ .<sup>33,55</sup> Again, it is the surface layer of the film that is the most accelerated in time scale.<sup>55,57</sup> Similarly, the stability of the glassy state quantified by the physical aging rate  $\beta(T)$  has also been found to change in thin films in a manner consistent with local  $T_g$  shifts at the interfaces.<sup>31,42,70–73</sup> An inspection of the temperature dependence of  $\beta(T)$  has shown that the aging response of the film is not simply consistent with a shift in the average  $T_g(h)$  of the film, but that the reduced aging rate in thinner films is consistent with their being a region with reduced local  $T_g$  at the free surface.<sup>42,70</sup> The one measure of a local aging rate in PMMA, again using a fluorescent dye, has shown reduced aging near the free surface consistent with the notion that a more liquid-like layer would age less, as well as reduced aging near the substrate interface attributed to a suppression of dynamics from hydrogen bonding with the substrate interface.<sup>74</sup> Most surprising is the long length scale of  $\sim 200$  nm, over which the interfacial perturbations appears to perturb these glassy aging dynamics.

Several studies have also investigated the density of thin films in the hopes of observing a decrease in density that could explain the large reductions in  $T_g$  observed. Such measurements are extremely challenging because the expected density changes that would correlate with the observed  $T_g(h)$  shifts are expected to be  $\sim 0.5\%$  or less,<sup>75,76</sup> which in many cases is within the experimental error of such a measurement.<sup>77,78</sup> To complicate matters, several recent studies have reported large  $\sim 25\%$  increases in density with decreasing film thickness,<sup>79–81</sup> which are unphysical. Efforts to decipher this contradictory behavior suggest that non-uniform polarizability within the thin film, possibly due to the observed dynamical gradients, may be complicating standard data analysis methods.<sup>82,83</sup>

Modulus is another property that has shown deviations from bulk in thin films. Measurements of thin glassy films at room temperature have shown decreases in the film's glassy modulus with decreasing film thickness in accordance with  $T_g$  changes from the free surface.<sup>84–88</sup> Notably, Vogt explains in his review that the change in glassy modulus with decreasing film thickness is not consistent with a simple shift of the master  $E(t, T)$  curve corresponding to the shift in average  $T_g(h)$  of the film, but instead the thin film behaves as "a graded composite material with low modulus near the free surface and thus a more significant decrease in modulus on confinement than if confinement led to uniform properties through the film thickness".<sup>84</sup> However, he cautions that this is only observed if the soft free surface region of the film is being probed by the measurement. Seemingly contradic-

tory to these observations of surface softening are the reports by McKenna's group of stiffening of the film in the rubbery region of the mechanical spectrum.<sup>89–91</sup> The understanding of how to reconcile these observations is still under discussion.<sup>92–95</sup> Given that modulus is a time and temperature dependent material property, ideally we want to gain a full understanding of how the mechanical response is altered in thin films near interfaces. The closest information like this we have at present is from nanoparticle embedding studies by McKenna and coworkers where the compliance  $J(T)$  of the near surface region has been extracted showing a softening in the glassy regime and a hardening in the rubbery regime.<sup>49,96</sup>

The picture of interfaces perturbing the local dynamics that then propagate deeper into the material has influenced the interpretation of many studies. Even when only a film average property is being measured, often the analysis of how the property changes as a function of film thickness involves a model that assumes some interface perturbation with bulk-like dynamics deeper in the film. To keep the model tractable, frequently a simplified layer model is used that breaks the film up into an interface layer of a certain thickness with an interior bulk-like layer. Experimentally if a single film average property is being measured, then the analysis can only extract a single parameter value from the model such that assumptions must be made about the properties of the interface layers.<sup>31</sup> For example, a common two-layer model assumes a liquid-like free surface layer atop a layer with bulk-like dynamics, where analysis of the changing film average property with decreasing film thickness is used to extract an effective layer thickness for this liquid-like free surface layer. Such an analysis typically gives mobile surface layer thicknesses of a few to several nanometers.<sup>25,55,70,97,98</sup> How one chooses to define the free surface layer, as either a liquid-like layer or simply a layer with enhanced dynamics faster than that of the bulk, will influence the identified thickness of this 'enhanced mobile layer', as well as its temperature dependence.<sup>10,66,99</sup> Interestingly, there also appears to be some upper-bound temperature well above  $T_g^{\text{bulk}}$ , above which no confinement effects are observed.<sup>50,100,101</sup>

Thus, the nature of the gradient in dynamics near the free surface is still not completely clear. To what extent the free surface mobile layer is actually liquid-like for a measurement at a given temperature and to what depth will depend on what is being probed. Studies commonly report surface mobile layer thicknesses that can on first consideration appear contradictory if consideration of what is being measured is not considered. Let's make a comparison of two different reported length scales for the same system of supported PS films and see how we can rationalize this apparent discrepancy. Several free surface studies utilize some measure of surface diffusion, relaxation, or flow to identify a liquid-like length scale. We focus here on one particularly comprehensive study by Qi and Forrest where the mobility of PS chains at the free surface were studied by measuring the embedding or sinking of small gold nanoparticles into the film.<sup>56</sup> The range of PS molecular weights studied varied from 3 kg/mol to 1210 kg/mol. For low molecular weights  $M_w \leq 22.2$  kg/mol, surface diffusion of the oligomeric chains readily occurred engulfing the nanoparticles. Similar surface diffusive flows are observed

in small molecules demonstrating an accelerated surface dynamics.<sup>102–105</sup> For higher molecular weights  $M_w \geq 86.8$  kg/mol, the nanoparticles were able to embed into the first  $\sim 5$  nm of the surface, even at temperatures 16.5 K below  $T_g^{\text{bulk}}$ , with no molecular weight dependence observed.<sup>56</sup> Sinking further into the film required temperatures comparable to  $T_g^{\text{bulk}}$ , where penetration was limited by the slow shifting of local entanglement points to accommodate the 16–30 nm diameter nanoparticles, again a process found to be independent of molecular weight. The authors concluded that the PS films for the entire range of molecular weights studied from 3 to 1210 kg/mol exhibited a 4–8 nm thick free surface layer that was liquid like. The differing behavior of the low and high molecular weight films occurred because the low molecular weight chains were small enough in size to exist entirely within this liquid-like surface region and therefore free to diffuse laterally across the surface of the film like small molecules, while the larger molecular weights had some portion of their chain anchored into the deeper, glassy region of the film limiting their diffusion. How do we reconcile this 4–8 nm thick liquid-like surface layer with the local  $T_g$  results presented in Figure 2? These were also supported PS films, with molecular weights  $M_w = 425$  to 760 kg/mol, where the fluorescence measurements indicated that bulk  $T_g$  was not recovered until a depth of  $\approx 30$  nm into the film. We can reconcile these two different length scales by recognizing that there is likely a continuous gradient in dynamics with depth as indicated by the local  $T_g$  profile shown in Fig. 2, where the first few nanometers of the film are effectively liquid-like, although still highly viscous, followed by a glassy region with a reduced  $T_g$ , until bulk dynamics are finally recovered deeper into the material. As experimentally there is no molecular weight dependence observed in either measurement, it would appear that the depth-dependent gradient in local dynamics is largely the same for all molecular weights.

Some successful interpretations of changing dynamics in thin films have been made by treating the free surface region as simply existing at a higher rheological temperature relative to the sample temperature, such that the gradient in dynamics near the free surface is effectively a gradient in local temperature.<sup>106</sup> Theoretical efforts that treat the free surface need to model the magnitude of the enhanced mobility explicitly. Frequently this is done by treating the free surface as having some fraction of missing contacts, which then makes local molecular rearrangements easier to occur.<sup>76,107</sup> Perhaps one of the most remarkable demonstrations that the free surface has significant additional mobility is the ability to form so-called "stable glasses" by physical vapor deposition.<sup>108,109</sup> By depositing glass forming molecules at temperatures only a few tens of degrees below their  $T_g$ s at a slow enough rate, the freshly deposited surface layer of molecules has sufficient extra mobility that molecular packing can be optimized before the next layer of molecules is deposited. In this way, films of stable glasses can be formed that have  $\approx 1$ –2 % higher density than an ordinary temperature-cooled glass, effectively producing glasses that are equivalent to ones that have been physically aged for 10,000 years or more.<sup>108,110</sup>

The nature of the free surface appears to be particularly unique. Efforts have been made to measure films with polymer–liquid in-



interfaces because it was initially thought that such an interface could be similar to a free surface.<sup>111,112</sup> However, surprisingly that has turned out not to be the case. Measurements of PS films floating on the surface of glycerol or an ionic liquid have found the behavior of the film average  $T_g(h)$  to be equivalent to that for a PS film supported on silicon,<sup>112–114</sup> suggesting the polymer–liquid interface is more analogous to a polymer–substrate interface.

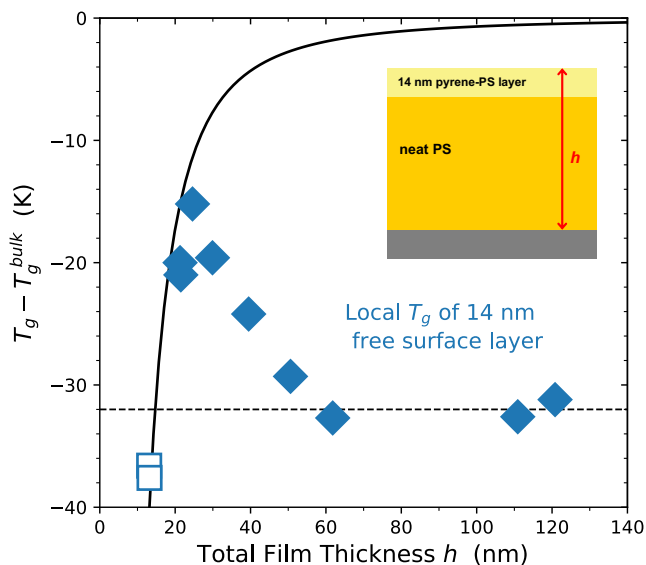


**Fig. 4** Local  $\Delta T_g = T_g - T_g^{\text{bulk}}$  for 14-nm thick pyrene-labeled PS free surface probe layer as a function of total PS film thickness. Diamonds are for probe layers placed at the free surface atop neat PS films supported on silica, while the open squares give the average  $T_g(h)$  for 14-nm thick films. The black curve represents the  $T_g(h)$  data for PS films measured by fluorescence as fit by Eq. 1. [Data replotted from Ref. 19.]

Although it is clear that the source of the property changes in nanoconfined films is caused by interfacial perturbations, the situation of understanding these behaviors is not quite as simple as only summing the various interfacial interactions. The overall film thickness can also affect the measured dynamics at the interface indicating that ‘cross-talk’ between interfaces at the top and bottom of the film occurs, sometimes over remarkably long length scales  $\sim 200$  nm.<sup>19,115</sup> Figures 4 and 5 show two such examples of this behavior. Figure 4 plots the local glass transition temperature reduction  $\Delta T_g = T_g - T_g^{\text{bulk}}$  as measured by a pyrene-labeled probe layer for a 14-nm thick free-surface layer of PS as a function of total film thickness.<sup>19</sup> Remarkably, the  $\Delta T_g$  reduction is only constant at  $-32$  K for total film thicknesses  $h \geq 60$  nm. Below 60 nm, the free surface layer  $T_g$  increases to  $\Delta T_g = -15$  K for  $h = 25$  nm films where it merges with the average  $T_g(h)$  reduction observed for the entire film. Ellison and Torkelson described this as suggesting that some minimum total film thickness may be required to maintain such a large gradient in dynamics.<sup>19</sup> After all, an  $\approx 30$  K difference in local  $T_g$  implies a gradient in local relaxation time scales  $\Delta\tau_\alpha \sim 10^7$  s.

Figure 5 compares the surface relaxation time at  $T_g^{\text{bulk}} - 36$  K for small ‘nanohole’ indentations at the surface of isotactic PMMA films supported on either silica or Al substrates as a function of the

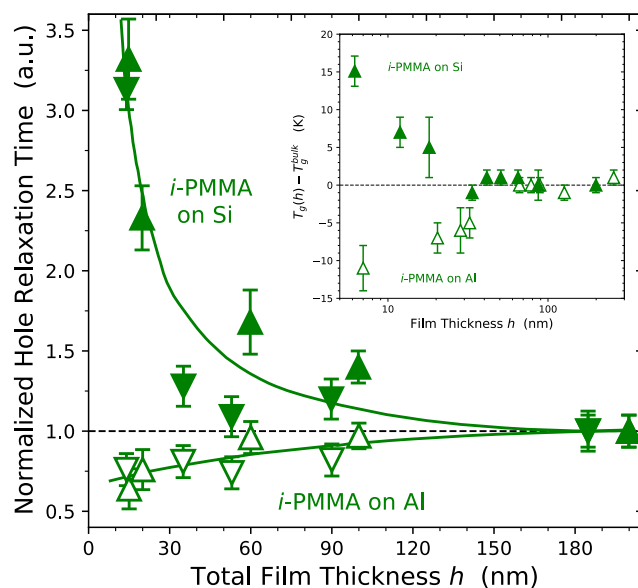


**Fig. 5** Normalized hole relaxation time for small ‘nanohole’ indentations at the free surface of isotactic PMMA films as a function of total film thickness  $h$ . Solid symbols are  $i$ -PMMA films supported on silicon wafers with native oxide layers, while open symbols are supported on Al substrates:  $M_w = 212.4$  kg/mol (upward pointing triangles),  $M_w = 889$  kg/mol (downward pointing triangles). Inset shows the  $T_g(h)$  dependence for  $M_w = 212.4$  kg/mol  $i$ -PMMA films on silicon and Al substrates. [Data replotted from Ref. 115,116.]

total film thickness.<sup>115</sup> These data by Qi, Fakhraai, and Forrest show that the surface relaxation time of these supported  $i$ -PMMA films are only equivalent for film thicknesses greater than 180 nm. The inset gives the  $\Delta T_g(h) = T_g(h) - T_g^{\text{bulk}}$  behavior for this polymer on these two different substrates indicating that silica substrates are attractive, while Al substrates are not.<sup>116</sup> Thus, some aspect of the slower dynamics caused by the attractive  $i$ -PMMA–silica interactions must be influencing the surface relaxations over remarkably long distances through the mostly glassy film. The effect is the same for both molecular weights studied,  $M_w = 212.4$  kg/mol ( $R_g \approx 12$  nm) and  $M_w = 889$  kg/mol ( $R_g \approx 25$  nm), indicating that some long range interaction goes far beyond chain size. It is these long-range ‘cross-talk’ interactions between interfaces that are the most puzzling.

### 3 Local $T_g$ Near and Across Dissimilar Polymer-Polymer Interfaces

Polymer-polymer interfaces between two different polymers, especially when they have strongly differing bulk  $T_g$ s, provide another avenue for the study of how interfacial perturbations alter local properties in materials. Such polymer–polymer interfaces are distinct from a polymer free surface, polymer–substrate interface, or even a polymer–liquid interface in several key respects. Most notably, polymer chains interpenetrate across the interface, intermixing locally, creating a broader interfacial width over which the composition profile changes ( $\sim 5$  nm) in comparison to the local density or composition profile at a polymer free surface or polymer–liquid interface (typically  $\sim 0.5$  nm).<sup>117</sup> The interfacial width formed between two immiscible polymers re-

sults from an energy balance between the entropic gain for chains to stretch out across the interface and the enthalpic energy cost of forming more unfavorable monomer–monomer contacts between the two different polymers. For high molecular weight polymers, this balance leads to a composition profile<sup>118</sup>

$$\phi(z) = \frac{1}{2} \left[ 1 + \tanh \left( \frac{2z}{w_I} \right) \right] \quad (5)$$

with a well-defined interfacial width  $w_I$  that depends on the interaction parameter  $\chi$  between the two polymers,

$$w_I = \frac{2b}{\sqrt{6\chi}}, \quad (6)$$

for polymers with comparable statistical segment lengths  $b$  and densities.

Despite these differences, there is no reason to believe that the underlying physics of the nanoconfinement phenomenon is any different: some perturbation to the dynamics at the interface that propagates away from the interface into the material creating a local gradient in properties. The specific differences associated with polymer–polymer interfaces likely only modifies the local behavior near the interface, and thus, by comparison with other types of interfaces, can be informative of the underlying factors that are important. And as we shall see, some of the differences associated with polymer–polymer interfaces can be replicated by modifying other types of interfaces, e.g., a polymer–substrate interface.

Early work from the Torkelson group found that the local  $T_g$  of 14-nm thick PS free surface layers could be strongly impacted by changing the underlying polymer,<sup>119–121</sup> demonstrating that the local  $T_g$  of the thin PS surface layer could be nearly slaved to the bulk  $T_g$  of an underlying polymer.<sup>121</sup> Similarly, differences in the temperature-dependent shift factor  $\log(a_T)$  of 20-nm thick PS free surface layers atop bulk PS, PMMA, and P2VP underlayers were also observed by Yoon and McKenna using nanoparticle embedding.<sup>122</sup> Rauscher et al. showed that the  $T_g(h)$  reduction of PS films supported on soft rubbery poly(*n*-butyl methacrylate) (PnBMA) underlayers had larger  $T_g(h)$  reductions than PS films supported on silica, demonstrating that the glassy-rubbery PS/PnBMA interface was contributing an additional source of enhanced mobility.<sup>123</sup> The layer average  $T_g$  of nanolayered films with many alternating glassy-rubbery layers were found to be strongly perturbed by the increasing amount of interfacial material present as layer thicknesses were reduced.<sup>124–126</sup> Theoretical efforts were also beginning to tackle interfaces between two different polymer domains.<sup>127,128</sup>

It was these early studies demonstrating the strong impact of polymer–polymer interfaces on local properties, but where the interpretation of  $T_g$  shifts was typically complicated by competing interactions from multiple interfaces, that motivated the investigation of a system with a single polymer–polymer interface. Consider the system shown in Figure 6a of two semi-infinite polymer domains forming a single polymer–polymer interface between a glassy polymer with a much higher  $T_g^{\text{bulk}}$  (PS  $T_g^{\text{bulk}} = 100$  °C) and a rubbery polymer with a much lower  $T_g^{\text{bulk}}$  (PnBMA  $T_g^{\text{bulk}}$

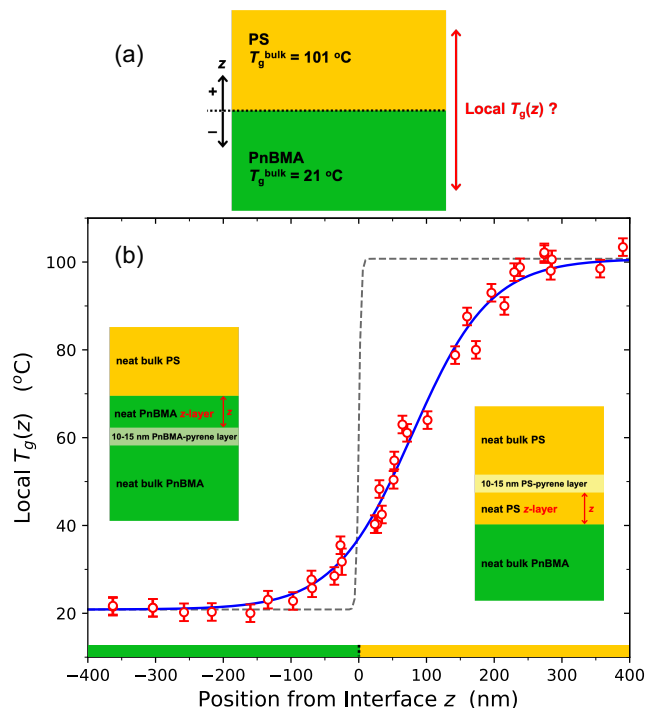


**Fig. 6** (a) Schematic of the glassy-rubbery polymer-polymer interface between a bulk domain of PS ( $T_g^{\text{bulk}} = 101$  °C) and a bulk domain of PnBMA ( $T_g^{\text{bulk}} = 21$  °C) indicating the  $z$ -axis coordinate. How does the local glass transition temperature  $T_g(z)$  change from one bulk value to another? (b) Plot of the local  $T_g(z)$  measured by a localized pyrene-labeled probe layer placed at different positions from the PS/PnBMA interface. Blue curve is the hyperbolic tangent fit of Eq. 7 through the fluorescence data. Gray dashed curve would be the expected profile if the local  $T_g$  followed the composition profile  $\phi(z)$  given by Eq. 5 with the PS/PnBMA equilibrium interfacial width  $w_I = 7$  nm. [Data replotted from Ref. 129.]

$= 20$  °C). How will the local  $T_g(z)$  change across this interface? Obviously, far from the interface on either side, the  $T_g^{\text{bulk}}$  of that polymer must be recovered. Thus, somewhere across the interface the local  $T_g$  must transition the 80 K difference in bulk  $T_g$ s between these two polymers. The question is, how will this gradient in local  $T_g$  near the vicinity of the interface change from one polymer domain to the next?

Using the localized fluorescence method we can construct samples where a thin (10–15 nm) pyrene-labeled PS or PnBMA probe layer is placed at different positions  $z$  from the PS/PnBMA interface by inserting a spacer layer of neat polymer with a thickness  $z$  between the probe layer and the interface. The top and bottom neat polymer layers are made sufficiently thick ( $>450$  nm) such that the probe layer is not also affected by competing interactions from the free surface or substrate interface. Cartoons of such sample geometries are illustrated in Figure 6b, where we have defined the distance  $z$  from the polymer-polymer interface to be positive within the glassy PS domain and negative within the rubbery PnBMA domain. PS and PnBMA are weakly immiscible polymers such that when the polymer–polymer interface is annealed to equilibrium, the interfacial width between the two domains made of high molecular weight polymers is defined by Eq. 6 giving  $w_I = 7$  nm.<sup>123,130</sup> The success of this measurement



relies on using high molecular weight polymers and knowledge of the physics of polymer-polymer interface formation<sup>118,131,132</sup> to choose specific annealing conditions (described in detail in the original paper<sup>129</sup>) to create samples where the PS/PnBMA interface has been annealed to equilibrium, while still limiting the interdiffusion of the pyrene-labeled probe layer to keep it localized at the position  $z$ .

Figure 6b graphs the local  $T_g(z)$  profile measured by Baglay and Roth on either side of the PS/PnBMA interface using the localized fluorescence method on these carefully annealed multilayer samples. For this semi-infinite system, the  $T_g(z)$  profile is observed to be very broad, spanning 350–400 from one  $T_g^{\text{bulk}}$  value to the next, and surprisingly asymmetric relative to the composition profile, penetrating further into the glassy PS domain.<sup>129</sup> The  $T_g(z)$  data were found to be fit well by a hyperbolic tangent of the form

$$T_g(z) = T_g^{\text{av}} + \frac{1}{2} \Delta T_g \tanh \left[ \frac{2(z - \gamma)}{w} \right], \quad (7)$$

where the average  $T_g^{\text{av}} = \frac{1}{2}(T_g^{\text{bulk}}_{\text{PS}} + T_g^{\text{bulk}}_{\text{PnBMA}}) = 60.8$  °C and difference  $\Delta T_g = T_g^{\text{bulk}}_{\text{PS}} - T_g^{\text{bulk}}_{\text{PnBMA}} = 79.9$  K in  $T_g^{\text{bulk}}$  values were determined from the asymptotic limits of the data at large  $|z|$ , leaving only two fitting parameters to describe the  $T_g(z)$  profile, the width  $w = 231 \pm 5$  nm and asymmetry  $\gamma = 79 \pm 3$  nm.<sup>129</sup>

The breadth of this gradient in local  $T_g$  values is far broader than any expectation we may have from the prevailing paradigm associated with understanding  $T_g$  in polymer blends. The compositional dependence of the glass transition in polymer blends  $T_g(\phi)$  has typically been treated as depending on only the local composition  $\phi$  within a small region of order the Kuhn length (few nanometers).<sup>133–135</sup> From this viewpoint, we would have expected the  $T_g(z)$  profile across the PS/PnBMA interface to closely follow the compositional profile  $\phi(z)$  (Eq. 5). Within the 7-nm interfacial region monomers from both polymers are locally intermixed, while further away ( $|z| \gtrsim 10$  nm) only monomers of either PS or PnBMA are present. If the local  $T_g(z)$  depended only on composition, we would have expected a sharp transition in local  $T_g$  at the interface, illustrated by the gray dashed curve in Fig. 6b. However, from the  $T_g(z)$  data shown in Fig. 6b, we can clearly see that the local  $T_g(z)$  at  $z = 100$  nm, sufficiently far from the PS/PnBMA interface that only PS segments are present, is still significantly reduced from the  $T_g^{\text{bulk}}$  value of PS:  $T_g(z \approx 100 \text{ nm}) \approx T_g^{\text{bulk}}_{\text{PS}} - 30$  K. We also note that  $z = 100$  nm is sufficiently far away from the interface that individual chains are not spanning the distance. Control studies have verified that the local  $T_g(z)$  reductions are not caused by plasticization effects from short PnBMA chains migrating across the interface, with the local  $T_g(z)$  values measured being independent of the molecular weight and polydispersity of the chains provided the chains are long enough to prevent large scale diffusion of the probe layer.<sup>129,136,137</sup>

From the understanding of local  $T_g$  gradients near interfaces in nanoconfined systems described in Section 2, we know that the local  $T_g$  depends on more than just composition. Extra local mobility, for example at a free surface, can penetrate deeper into the material creating a local  $T_g(z)$  profile strongly reduced

from the bulk value (e.g., as illustrated in Fig. 2). It is possible that the polymer-polymer interface with the rubbery PnBMA is similarly imparting extra local mobility to the glassy PS domain that penetrates deeply into the glassy PS domain creating a large gradient in local  $T_g(z)$ . Tito, Lipson, and Milner have modeled such profiles in local mobility near free surfaces and between glassy-rubbery domains using a “limited mobility” three-state kinetic lattice model.<sup>128</sup> Intriguingly, these theoretical predictions of local mobility profiles  $\bar{\psi}(z)$  across glassy-rubbery-glassy slabs show a similar asymmetry to the experimental  $T_g(z)$  profile shown in Fig. 6b, penetrating deeper into the glassy domain.

The major difference between these theoretical predictions and the experimental results is the large difference in length scale. One likely factor causing this discrepancy is the breadth of the interface. While the theoretical study has an infinitely sharp interface, experimentally the interface between PS/PnBMA is very broad at  $w_I = 7$  nm. Follow up work by Baglay and Roth in 2017 demonstrated similarly broad and asymmetric  $T_g(z)$  profiles between PS and a series of different polymers that are all weakly immiscible with interfacial widths  $w_I = 5$ –7 nm.<sup>117</sup> These data from Ref. 117 of the local  $T_g(z)$  profile within PS next to polysulfone (PSF), PMMA, poly(isobutyl methacrylate) (PiBMA), PnBMA (data from Fig. 6b), along with additional data from Ref. 136 of PS next to polybutadiene (PB) are plotted in Figure 7. The asymmetry of the  $T_g(z)$  perturbation penetrating further into the glassy side can be observed by noticing how all the data extend to the same distance of  $z \approx 225$ –250 nm for  $T_g^{\text{bulk}}$  to be recovered within PS when next to softer polymers with lower  $T_g^{\text{bulk}}$  values: PiBMA ( $T_g^{\text{bulk}} = 62$  °C), PnBMA ( $T_g^{\text{bulk}} = 21$  °C), and PB ( $T_g^{\text{bulk}} = -96$  °C). In contrast, when PS is the softer polymer making an interface with a harder polymer with higher  $T_g^{\text{bulk}}$  value, PSF ( $T_g^{\text{bulk}} = 186$  °C) and PMMA ( $T_g^{\text{bulk}} = 120$  °C), the  $T_g(z)$  profile data recover  $T_g^{\text{bulk}}$  at a shorter distance of  $z \approx 100$ –125 nm. Interestingly, the  $T_g(z)$  profile within the softer PnBMA side from Fig. 6b is also consistent with this shorter penetration distance of  $z \approx 100$ –125 nm before  $T_g^{\text{bulk}}$  of PnBMA is recovered. This suggests that the penetration depth of the  $T_g(z)$  perturbation from the interface is not particularly dependent on chemical structure, but instead on whether the interface is made with a softer or harder polymer. Recent data from Gagnon and Roth have shown that the penetration depth of the  $T_g(z)$  profile within glassy PS can be significantly reduced to  $z \approx 65$ –90 nm when PS is paired with a much more immiscible polymer, rubbery polydimethylsiloxane (PDMS), resulting in a considerably narrower interfacial width  $w_I \approx 1.5$  nm.<sup>137</sup> These data also demonstrated that the magnitude of the  $T_g(z)$  reduction within PS could be controlled by varying the modulus of the neighboring PDMS domain.

The significance of the interface formed between the two dissimilar polymers to controlling and developing the broad and asymmetric  $T_g(z)$  profile across the glassy-rubbery interface was further confirmed by Baglay and Roth in 2017 by comparing  $T_g(z)$  values within PS next to PSF for samples where the annealing time to form the PS/PSF interface was varied.<sup>117</sup> To form an equilibrium interface between PS ( $T_g^{\text{bulk}} = 101$  °C) and PSF ( $T_g^{\text{bulk}} = 186$  °C), whose interfacial width  $w_I$  will be determined by Eq. 6, annealing must be done above the bulk  $T_g$  of both poly-

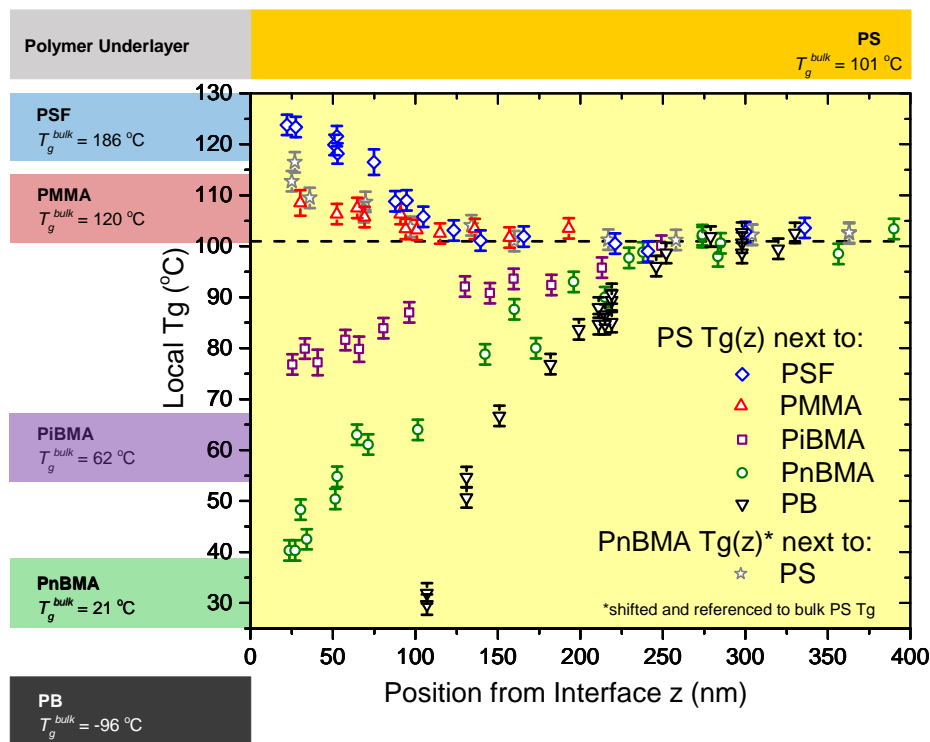


**Fig. 7** Local  $T_g(z)$  profiles within PS next to a series of different weakly immiscible polymers (interfacial widths  $w_I = 5\text{--}7$  nm) showing how  $T_g^{\text{bulk}}$  values are recovered only at a distance of  $z \approx 225\text{--}250$  nm when PS is next to softer polymers with lower  $T_g^{\text{bulk}}$  values (PiBMA, PnBMA, and PB) or a distance of  $z \approx 100\text{--}125$  nm when PS is next to harder polymers with higher  $T_g^{\text{bulk}}$  values (PSF and PMMA). The  $T_g(z)$  profile within rubbery PnBMA next to glassy PS from Fig. 6b is also consistent with this shorter penetration depth (gray stars, shifted and referenced to PS  $T_g^{\text{bulk}}$  for comparison). [Figure reproduced with permission from Ref. 136: "Local Glass Transition Temperature  $T_g(z)$  Profile in Polystyrene next to Polybutadiene With and Without Plasticization Effects," B. L. Kasavan, R. R. Baglay, and C. B. Roth, *Macromolecular Chemistry and Physics* **2018**, 219 (3), 1700328, Copyright © 2017 WILEY-VCH Verlag GmbH & Co. KGaA, Weinheim.]

mers.<sup>118,138</sup> To accomplish this, while still keeping the pyrene-labeled PS probe layer localized, the PS/PSF multilayer samples were annealed in two stages.<sup>117</sup> During the first stage, the neat PS  $z$ -spacer layer atop the bulk PSF domain were annealed together on their own at  $210$  °C ( $\approx 20\text{--}25$  K above the higher  $T_g^{\text{bulk}}$  value) until an equilibrium PS/PSF interface was formed (90 min). The second stage then added the pyrene-labeled PS probe layer and bulk neat PS layer on top, and annealed the complete sample geometry for only a further 5 min at  $170$  °C prior to the start of the fluorescence measurements. By varying the annealing time of the PS/PSF interface at  $210$  °C during the first stage, Baglay and Roth demonstrated how the  $T_g(z)$  profile developed as the interface between PS and PSF formed. Figure 8 graphs this process where the annealing time at  $210$  °C was progressively increased from 20 to 300 min, showing how  $>60$  min was required for the  $T_g(z)$  ( $z \approx 50$  nm) to saturate at a constant reproducible value of  $\approx 120$  °C. Figure 8b illustrates how the  $T_g(z)$  profile in PS next to the PS/PSF interface develops with this progressive amount of annealing of the PS/PSF interface to equilibrium. It would appear that without this crucial first annealing stage above the bulk  $T_g$  of both polymers, the  $T_g(z)$  profile would be rather sharp with the local  $T_g(z)$  within the PS domain being almost entirely equivalent to the  $T_g^{\text{bulk}}$  of PS.

These annealing studies demonstrate that formation of the dissimilar polymer-polymer interface to its equilibrium state is required for the glass transition dynamics to couple across the interface. This informs us about the underlying physics behind this phenomenon and indicates what factors may be important in controlling this behavior. The physics of polymer interface formation involves the interpenetration of chains across the interface leading to a broadening of the interface until an equilibrium width is

reached that balances the free energy changes from the entropic stretching of the chains with the formation of more unfavorable immiscible monomer–monomer contacts.<sup>118</sup> The presence of capillary waves also roughens the interface. If we compare the nature of polymer-polymer interfaces relative to other types of interfaces (polymer–free surface, polymer–substrate, and polymer–liquid), we can consider how these three factors could contribute to the broad  $T_g(z)$  profiles observed across dissimilar polymer-polymer interfaces.

- (i) *Breadth of interfacial region:* The local density profile at a free surface or liquid interface is typically quite sharp with interfacial widths  $\sim 0.5$  nm,<sup>139</sup> in contrast to polymer-polymer interfaces that typically have equilibrium interfacial widths of  $\sim 5$  nm,<sup>117,118,129</sup> an order of magnitude larger. We have already discussed how recent  $T_g(z)$  profiles measured by Gagnon and Roth for PS/PDMS, a strongly immiscible polymer pair with an interfacial width that is several times smaller than the broad interfacial widths of the weakly immiscible polymer pairs shown in Figure 7, resulted in a strongly reduced extent of the  $T_g(z)$  profile.<sup>137</sup> For PS next to a soft interface, the weakly immiscible polymer systems with  $w_I = 5\text{--}7$  nm had the  $T_g(z)$  profile extend to  $z \approx 225\text{--}250$  nm before  $T_g^{\text{bulk}}$  was recovered,<sup>117,129</sup> while the PS/PDMS system with  $w_I \approx 1.5$  nm only extended to  $z \approx 65\text{--}90$  nm before recovering  $T_g^{\text{bulk}}$ .<sup>137</sup> In addition, the data shown in Figure 8 demonstrate that formation of the broad polymer-polymer interface was required to observe the extended  $T_g(z)$  profiles.<sup>117</sup> This demonstrates that the breadth of the interfacial region plays a strong role in impacting the range of the  $T_g(z)$  profile. Recent theoretical work by Mirigian and Schweizer supports this observation, where a com-

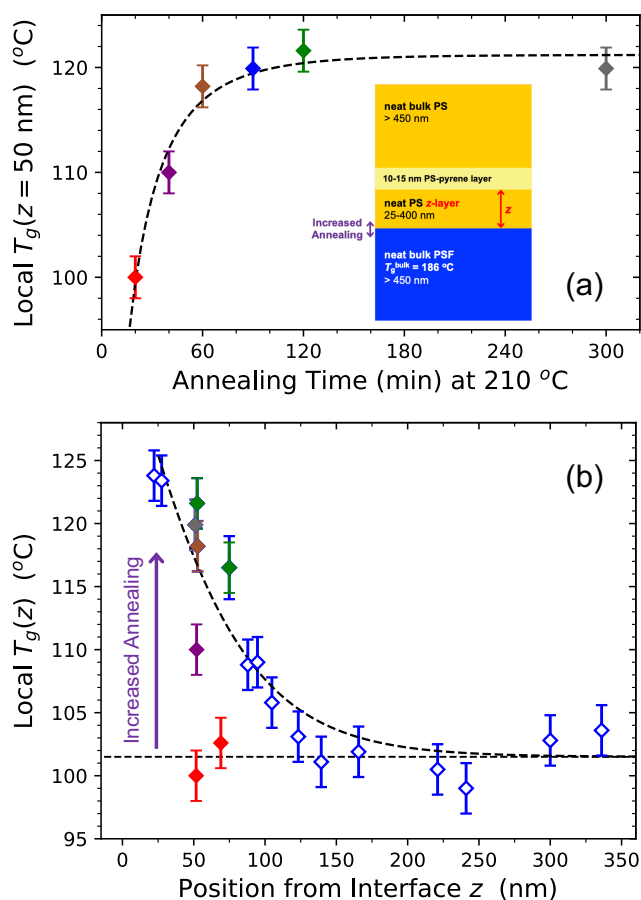


**Fig. 8** Demonstration of how the broad local  $T_g(z)$  profile within PS next to PSF ( $T_g^{\text{bulk}} = 186^{\circ}\text{C}$ ) develops as the PS/PSF interface is annealed to equilibrium at  $210^{\circ}\text{C}$ . (a) Local  $T_g(z=50 \text{ nm})$  as a function of time the PS/PSF interface was annealed showing  $>60 \text{ min}$  is required to reach equilibrium. (b) Local  $T_g(z)$  profile in PS next to PSF with the colored data corresponding to the same annealing times shown in (a): 20 min (red), 40 min (purple), 60 min (brown), 120 min (green), 300 min (gray), and 90 min (open blue symbols corresponding to the PS/PSF data shown in Fig. 7). [Data replotted from Ref. 117.]

comparison of the penetration depth of the locally perturbed dynamics near a free surface with their Elastically Collective Nonlinear Langevin Equation (ECNLE) theory showed an approximate doubling of the penetration depth when the local density profile at the free surface was modeled with a more realistic interfacial width of one particle diameter, instead of an artificially sharp step-change (infinitely narrow interface) that is computationally easier to implement.<sup>95</sup>

- (ii) *Chain connectivity across the interface*: In contrast to a free surface where surface tension prevents chain segments from poking out of the surface, polymer-polymer interfaces have chain connectivity across the interface. In general, chain connectivity does not strongly impact  $T_g$  in polymers for high molecular weight chains as the packing frustration associated with the glass transition is at the cooperative segmental level.<sup>140</sup> The local  $T_g$  measured by fluorescence is not impacted by changing molecular weight or polydispersity, provided the chain length is large enough to limit dif-

fusion and keep the probe layer localized.<sup>19,129,136</sup> Thus, as a first estimate, one would not anticipate this factor to have much impact.

- (iii) *Roughness of the interface*: The interfacial tension of polymer-polymer interfaces is approximately an order of magnitude less than the surface tension at a polymer-air surface.<sup>141</sup> This means that the amplitude of capillary waves  $\langle \zeta^2 \rangle \sim k_b T / \gamma$  at the interface due to normal thermal fluctuations ( $k_b$  is Boltzmann's constant and  $\gamma$  is the interfacial tension) will be approximately an order of magnitude larger at a polymer-polymer interface relative to that at a free surface resulting in a rougher interface.<sup>118,142</sup> How interface roughness might impact the local  $T_g$  near the interface is still an open question. Computational studies have long since demonstrated that the local  $\alpha$ -relaxation time  $\tau_\alpha$  next to an interface can be strongly influenced by whether the interface is smooth vs. rough.<sup>7,67,143-148</sup> However, experimentally the impact of interface roughness has not been investigated until recently.<sup>149-152</sup>

Huang and Roth carried out a series of experiments aimed at separating and testing how these various factors impact local  $T_g$ .<sup>149,153</sup> By tethering PS chains to silica substrates a sharp, flat interface can be created that isolates only the effects of chain connectivity to the interface (ii), alternatively by roughening silica substrates, a sharp interface with no chain connectivity can be investigated to isolate the impact of interface roughness (iii). In both cases a fluorescent probe layer was placed next to or near the interface to measure the local  $T_g$ , while crucially, a neat bulk ( $>500 \text{ nm}$ ) PS layer was placed on top to avoid competing effects from the free surface. From these studies, it was observed that end-tethered chains at low grafting densities produced a large, 40–50 K increase in local  $T_g$  and resulted in  $T_g(z)$  profiles next to the end-tethered interface that was very similar to those seen for polymer-polymer interfaces.<sup>153</sup> In contrast, roughening silica substrates led to little to no change in local  $T_g$  next to the interface, at most only a 10 K increase in local  $T_g$  for extremely rough surfaces.<sup>149</sup> Thus, we can conclude that (ii) chain connectivity to the interface plays a surprisingly important role.

Figure 9 graphs the local  $T_g(z)$  profiles measured by Huang and Roth next to PS end-tethered silica substrates with different grafting densities.<sup>153</sup> These fluorescence measurements were done by creating samples where PS-COOH ( $M_w = 101.8 \text{ kg/mol}$ ,  $M_w/M_n = 1.03$ ) chains were grafted to silica substrates at low grafting densities  $\sigma = 0-0.042 \text{ chains/nm}^2$ . A neat  $z$ -spacer layer was then added to vary the distance from the interface to a 12-nm thick pyrene-labeled probe layer, followed by a neat bulk ( $>500 \text{ nm}$ ) PS layer to eliminate competing effects from the free surface. To measure the local  $T_g(z=0)$  right next to the interface, the  $z$ -spacer layer was not included. Based on the importance of intermixing and annealing the interface to equilibrium shown in Figure 8, care was taken to intermix the grafted chains with the first layer added by performing a first annealing stage of only these two layers for 2 h at  $170^{\circ}\text{C}$ ,<sup>153-155</sup> prior to adding the remaining sample layers.

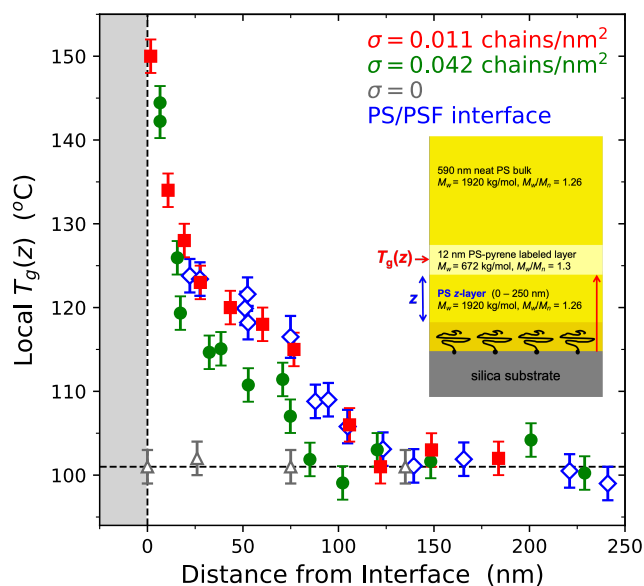


**Fig. 9** Local  $T_g(z)$  profile in PS next to a silica interface with PS end-tethered chains ( $M_w = 101.8$  kg/mol) with grafting density  $\sigma = 0.011$  chains/nm<sup>2</sup> (red),  $\sigma = 0.042$  chains/nm<sup>2</sup> (green), and zero grafted chains (gray). For comparison, the local  $T_g(z)$  profile in PS next to PSF ( $T_g^{\text{bulk}} = 186$  °C) from Fig. 7 is shown as blue data. [Data replotted from Ref. 153.]

The  $T_g(z)$  profiles for two different grafting densities  $\sigma = 0.011$  and  $0.042$  chains/nm<sup>2</sup> are shown in Figure 9. Based on measurements of the local  $T_g(z=0)$  for a range of grafting densities,  $\sigma = 0.011$  chains/nm<sup>2</sup>, within the mushroom-to-brush transition region, was found to show the largest local  $T_g(z=0)$  increase of  $49 \pm 2$  K above  $T_g^{\text{bulk}}$ , while  $\sigma = 0.042$  chains/nm<sup>2</sup> was the highest grafting density investigated.<sup>153</sup> As anticipated, silica substrates with no grafted chains ( $\sigma = 0$ ) did not perturb the local  $T_g$  from bulk (as shown in Fig. 3). Remarkably, the magnitude and extent of the  $T_g(z)$  profile for this “optimum” grafting density of  $\sigma = 0.011$  chains/nm<sup>2</sup>, showing the largest local  $T_g$  increase, is within experimental error identical to the  $T_g(z)$  profile measured for PS next to PSF, a “hard” neighboring polymer with a much higher  $T_g^{\text{bulk}}$  than PS. This strongly suggests that chain connectivity to the interface (factor ii) plays a strong role in influencing the local  $T_g(z)$  profiles, while interfacial roughness at the polymer-polymer interface has a negligible (if any) effect.<sup>149,153</sup> Note that similar to the polymer-polymer interfaces, the perturbation of the  $T_g(z)$  profile extends further than any given chain connected to the interface. For the  $T_g(z)$  profiles shown in Figure 9, the surface grafted chains extend only approximately  $2R_g = 17$  nm from the silica interface.<sup>153</sup> Thus, the underlying physics of why this chain connectivity to the interface has such a large impact on the local  $T_g(z)$ , beyond the extent of the individual chains themselves, remains an open question. What is clear is that the effect is largest at extremely low grafting densities where the grafted chains are able to easily interpenetrate with the neighboring untethered chains.

So far in this section, we have only discussed single polymer-polymer interfaces between semi-infinite domains where the in-

terfacial perturbation is free to propagate as far as needed before  $T_g^{\text{bulk}}$  is recovered. This is a simplified system useful for understanding the physics of the phenomenon. However, most applications involving polymer-polymer interfaces have many domains, either of a given size such as in microphase-separated block copolymers or of varying random sizes as in polymer blends. Clearly for most applications, it is important to understand how domains of a finite size with more than one polymer-polymer interface behave.

Let us consider a PnBMA/PS/PnBMA trilayer system where the two PnBMA layers are still sufficiently thick ( $>450$  nm) such that external interfaces with a free surface or underlying substrate do not cause additional perturbations. The middle PS domain is now sandwiched between two PS/PnBMA interfaces, each presumably exerting some  $T_g(z)$  perturbation on the PS layer similar to that shown in Fig. 6. If the two PS/PnBMA interfaces are far enough away from each other, one would expect each  $T_g(z)$  perturbation from either interface to act independent of each other with  $T_g^{\text{bulk}}$  recovered in the middle of the PS domain. Baglay and Roth investigated such a PnBMA/PS/PnBMA trilayer system, using fluorescence to measure the local  $T_g(z)$  at a fixed position  $z = 100$  nm from one interface, while systematically reducing the PS domain size.<sup>156</sup> They observed a further reduction in the  $T_g(z = 100$  nm) value due to the presence of the second PS/PnBMA interface when the total PS domain size reached less than  $\approx 400$  nm.

As shown in Figure 10, Baglay and Roth also mapped the local  $T_g(z)$  across a 300 nm PS domain sandwiched between two bulk PnBMA layers.<sup>156</sup> We can compare these experimentally measured values with what one might anticipate if the  $T_g$  reduction was a linear superposition of  $\Delta T_g$  changes from both interfaces. Figure 10 graphs the anticipated  $T_g(z)$  profile from the two separate PS/PnBMA interfaces (black dashed curves) based on the Eq. 7 fit to the data shown in Fig. 6, as well as the linear superposition of these two individual  $\Delta T_g$  perturbations as the green dashed curve. We can see that the experimentally measured  $T_g(z)$  data (blue symbols) are further reduced from this first order estimate. This suggests that the finite size of the PS domain further alters the  $T_g(z)$  perturbation. Perhaps accounting for perturbations from multiple interfaces requires summing some different quantity such as a local activation barrier<sup>157–159</sup> or other factor that controls the local  $\alpha$ -relaxations.<sup>128</sup> Clearly more work at reduced domain sizes are needed to better understand this behavior.

Evans et al. used fluorescence to measure the average  $T_g$  of PS domains sandwiched between between two bulk (500 nm) domains of different polymers: poly(4-vinyl pyridine) (P4VP) ( $T_g^{\text{bulk}} = 150$  °C), polycarbonate (PC) ( $T_g^{\text{bulk}} = 141$  °C), poly(vinyl chloride) (PVC) ( $T_g^{\text{bulk}} = 80$  °C), and poly(tert-butyl acrylate) (PtBA) ( $T_g^{\text{bulk}} = 42$  °C).<sup>121</sup> For sandwiched PS layer thicknesses less than  $\approx 100$  nm, the average  $T_g$  of the PS domain was found to shift towards the  $T_g^{\text{bulk}}$  value of the neighboring bulk polymer domains. For the thinnest 14-nm thick PS layers, the  $T_g$  values were found to be equivalent to those measured previously for isolated PS chains within nearly infinitely-dilute blends (0.1 wt%) with these same neighboring polymers as matrices.<sup>160</sup> The magnitude of the  $T_g$  shifts for the 14-nm thick PS domains towards that of

the neighboring bulk polymer domains was found to scale with the fragility  $m$  of the neighboring bulk polymer.<sup>121</sup>

Christie, Register, and Priestley have used fluorescence to measure the local  $T_g(z)$  across diblock copolymer lamellae domains of PnBMA-PMMA by covalently attaching the pyrene dye to different positions along the diblock copolymer backbone.<sup>161</sup> The local  $T_g(z)$  profile was found to show a remarkably strong gradient in excess of 60 K over only an 8 nm span, needing to fit within half the repeating domain period ( $d = 27$  nm for this PnBMA-PMMA diblock of  $M = 47$  kg/mol). This  $T_g(z)$  profile is also asymmetric, more strongly impacting the glassy PMMA domain, with the PMMA homopolymer  $T_g^{\text{bulk}}$  not being recovered within the narrow domains. A follow-up study that compared the  $T_g$  of fluorescently labeled PMMA homopolymer added at low concentrations to unlabelled PnBMA-PMMA diblocks concluded that chain connectivity of the diblock segments to the glassy-rubbery interface contributed a significant amount ( $\sim 10$  K) of the local  $T_g(z)$  reduction within the PMMA block copolymer domains.<sup>162</sup>

Alternating glassy/rubbery domain structures are also observed in nanolayered films made by a layer multiplying coextrusion technique that produces films with thousands of alternating polymer layers.<sup>124,125</sup> A study by Arabeche et al. used temperature

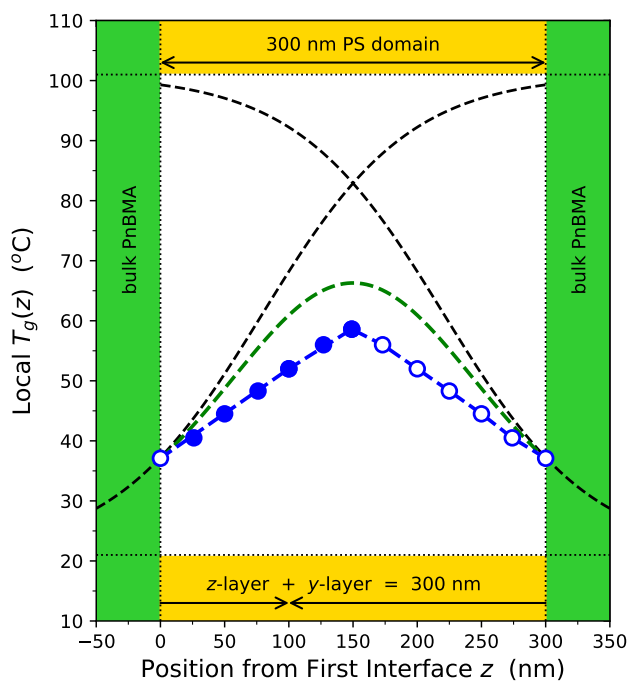


**Fig. 10** Local  $T_g(z)$  profile within a 300 nm PS domain sandwiched between two bulk ( $>450$  nm) PnBMA layers. Neat PS spacer layers of thickness  $z$  and  $y$ , below and above the 12-nm pyrene-labeled PS probe layer, were adjusted to keep a fixed total PS domain thickness of 300 nm. Fluorescence data collected at 1 K/min on cooling are shown as solid blue symbols, while the open symbols are obtained by mirroring the data about the mid-plane. The  $T_g(z=0)$  is interpolated from the data shown in Fig. 6. Black dashed curves represent the  $T_g(z)$  profile for a single interface based on Eq. 7, mirrored to show the potential  $T_g$  reduction from both interfaces. The green dashed curve represents the anticipated profile based on a linear superposition of  $\Delta T_g$  reductions from either interface. [Data replotted from Ref. 156.]

modulated differential scanning calorimetry (TMDSC) to study such films of alternating PC/PMMA layers.<sup>126</sup> As the layer thicknesses decreased, the individual glass transitions of the two polymers merged into a single broad transition for layer thicknesses of  $\approx 125$  nm and smaller. In particular, it was the transition of the glassy PC component that became more asymmetric, shifted and skewed towards the lower  $T_g$  PMMA component, consistent with the asymmetries observed in the  $T_g(z)$  profiles above. Similar glass transition broadening has been reported by Guar and Wunderlich using DSC to measure high molecular weight block copolymers of PS and poly( $\alpha$ -methyl styrene) (P $\alpha$ MS), a weakly immiscible system.<sup>163</sup> These high molecular weight (400-1700 kg/mol) block copolymers self-assembled into large lamellae domains with alternating layer thicknesses of 120/60 nm and 45/75 nm P $\alpha$ MS/PS. For these systems with large domain sizes, the observed glass transition was significantly broadened with the lower  $T_g$  PS component broadening to higher temperatures and the higher  $T_g$  P $\alpha$ MS component broadening to lower temperatures. A study of block copolymer systems with smaller domain sizes (20–70 nm) by Robertson et al. found that the magnitude of the  $T_g$  shift in the confined blocks' DSC transition depended on the relative immiscibility of the two components, as characterized by their difference in solubility parameters.<sup>164</sup> They concluded that in the limit of diverging solubility parameters of the two blocks, where the interface would become extremely sharp, no  $T_g$  shift would be expected. Thus, similar to the local  $T_g(z)$  fluorescence studies, these DSC studies suggest the breadth of the interface between the two domains is important for controlling the amount of  $T_g$  perturbation that is transmitted across the interface. The biggest  $T_g$  changes are observed when the interfacial regions between the domains are broad, with larger domains typically showing an asymmetric broadening of the glass transition, while smaller domains are interpreted more as a shift in  $T_g$ .

Addressing the impact of finite domain size on the local  $T_g(z)$  behavior is important not only for interpreting these measurements of the average glass transition behavior of nanostructured materials and those of other experimental techniques that are limited to global measurements of the sample, but also for making comparisons with computer simulations. The sizes of simulations are still limited by computational power, especially for the long time dynamics relevant to glass transition studies. As such, computer simulations utilize periodic boundary conditions to extend the simulation volume by wrapping the coordinates in a given direction back on itself. An example of the implications of this are the bead-spring simulations by Lang, Merling, and Simmons of a low  $T_g$  domain next to a high  $T_g$  domain.<sup>127</sup> Even though the simulation volume itself was simply these two low and high  $T_g$  domains, the use of periodic boundary conditions extended the domains laterally into layers, while normal to the interface, the use of periodic boundary conditions created a system with alternating low and high  $T_g$  layers akin to the nanolayered films described above. Certainly this is a valuable geometry for investigation. It is simply unfortunate that current limits in computational power prevent a semi-infinite system akin to Fig. 6 to be modeled. The results of the Lang, Merling, and Simmons simulation observed the largest  $T_g$  shifts when the breadth of the interface between



the low and high  $T_g$  layers was widest, where the strength of the shift was correlated with the Debye-Waller factor, proportional to the high frequency modulus, of the neighboring domain.<sup>127</sup> Less acknowledged in molecular dynamics simulations is that periodic boundary conditions also truncate any long-wavelength fluctuations beyond the simulation size,<sup>165</sup> which will inhibit the observation of any long-range effects.

## 4 Conclusions and Open Questions

This review has focused on localized measures of  $T_g$  primarily by fluorescence, with some discussion of average  $T_g$  measurements and other properties, to present a phenomenological picture of our current understanding of local glass transition changes in nanoconfined polymer systems. It is the hope that such information on these simplified systems with only one or two interfaces will prove useful in interpreting the behavior of more complex nanostructured materials with a multitude of interfaces. For readers interested in a theoretical description, a recent review by Schweizer and Simmons has provided an in-depth summary of the current state of this literature in thin films.<sup>3</sup>

By comparing and contrasting local  $T_g(z)$  changes near and across polymer-polymer interfaces with other types of interfaces, polymer-air free surface, polymer-substrate, and polymer-liquid, we can draw several conclusions. What appears to be unique about polymer-polymer interfaces is primarily due to its wider interfacial breadth, with chain connectivity across the interface likely playing an important role. Weakly immiscible systems with broad  $\sim 5$  nm interfacial widths exhibit remarkably long-range effects, which shorten significantly for strongly immiscible systems with interfacial widths  $\sim 1$ – $2$  nm.<sup>117,129,137</sup> In contrast, free surface and polymer-liquid interfaces have much narrower  $\sim 0.5$  nm interfacial widths. Annealing of the dissimilar polymer-polymer interface to equilibrium was required to observe the long-range  $T_g(z)$  profiles, where the extent of the perturbed dynamics before  $T_g^{\text{bulk}}$  was recovered depended on the hardness or softness of the neighboring polymer domain.<sup>117</sup> Surprisingly, chain connectivity to the interface appears to have a remarkably large impact extending far beyond the spacial extent of the chains tethered to the interface. In fact, the same  $T_g(z)$  profile as that next to a harder polymer domain with a higher  $T_g^{\text{bulk}}$  can be recreated by end-tethering chains to silica substrates at low grafting densities.<sup>153</sup> The underlying cause of this is still unknown as the packing frustration causing the glass transition in polymers is at the cooperative segmental level and not generally associated with chain connectivity.

A major open question remains about how multiple interfaces interact within a domain or film of finite size. Both thin films and multilayer samples with polymer-polymer interfaces indicate that long-range 'cross-talk' between interfaces can occur over distances  $\sim 200$ – $300$  nm.<sup>115,156</sup> Information is needed to bridge the gap between larger and smaller domain sizes to better understand the differences between local perturbations at single interfaces and systems with many alternating layers such as block copolymers,<sup>161,162</sup> as well as provide data for model systems that can be reasonably accessed with computer simulations.

## Conflicts of interest

There are no conflicts to declare.

## Acknowledgements

The author gratefully acknowledges support from the National Science Foundation Polymers Program (DMR-1905782 and DMR-1709132) and Emory University, as well as many excellent conversations with current and former students, and colleagues.

## References

- 1 D. R. Paul and C. B. Bucknall, *Polymer Blends: Formulation & Performance, Vol. 1*, Wiley, New York, 2000.
- 2 C. Harrats, S. Thomas and G. Groeninckx, *Micro- and Nanostructured Multiphase Polymer Blend Systems: Phase Morphology and Interfaces*, CRC Press, Boca Raton, FL, 2006.
- 3 K. S. Schweizer and D. S. Simmons, *Journal of Chemical Physics*, 2019, **151**, 240901.
- 4 J. A. Forrest and K. Dalnoki-Veress, *Advances in Colloid and Interface Science*, 2001, **94**, 167–195.
- 5 C. B. Roth and J. R. Dutcher, *Journal of Electroanalytical Chemistry*, 2005, **584**, 13–22.
- 6 M. Alcoutlabi and G. B. McKenna, *Journal of Physics: Condensed Matter*, 2005, **17**, R461.
- 7 J. Baschnagel and F. Varnik, *Journal of Physics: Condensed Matter*, 2005, **17**, R851.
- 8 M. D. Ediger and J. A. Forrest, *Macromolecules*, 2013, **47**, 471–478.
- 9 D. S. Simmons, *Macromolecular Chemistry and Physics*, 2016, **217**, 137–148.
- 10 C. B. Roth, J. E. Pye and R. R. Baglay, *Polymer Glasses*, CRC Press, Boca Raton, FL, 2016, ch. 5: Correlating Glass Transition and Physical Aging in Thin Polymer Films, pp. 181 – 204.
- 11 J. L. Keddie, R. A. L. Jones and R. A. Cory, *Europhysics Letters*, 1994, **27**, 59 – 64.
- 12 J. A. Forrest, K. Dalnoki-Veress, J. R. Stevens and J. R. Dutcher, *Physical Review Letters*, 1996, **77**, 2002–2005.
- 13 J. Mattsson, J. A. Forrest and L. Börjesson, *Physical Review E*, 2000, **62**, 5187–5200.
- 14 K. Dalnoki-Veress, J. A. Forrest, C. Murray, C. Gigault and J. R. Dutcher, *Physical Review E*, 2001, **63**, 031801.
- 15 J. E. Pye and C. B. Roth, *Physical Review Letters*, 2011, **107**, 235701.
- 16 J. E. Pye and C. B. Roth, *Journal of Polymer Science Part B: Polymer Physics*, 2015, **53**, 64 – 75.
- 17 J. S. Sharp and J. A. Forrest, *Physical Review Letters*, 2003, **91**, 235701.
- 18 J. S. Sharp, J. H. Teichroeb and J. A. Forrest, *European Physical Journal E*, 2004, **15**, 473–487.
- 19 C. J. Ellison and J. M. Torkelson, *Nature Materials*, 2003, **2**, 695 – 700.
- 20 C. J. Ellison, M. K. Mundra and J. M. Torkelson, *Macromolecules*, 2005, **38**, 1767 – 1778.



- 21 C. J. Ellison and J. M. Torkelson, *Journal of Polymer Science Part B: Polymer Physics*, 2002, **40**, 2745–2758.
- 22 S. Kim, S. A. Hewlett, C. B. Roth and J. M. Torkelson, *European Physical Journal E*, 2009, **30**, 83.
- 23 C. B. Roth and J. R. Dutcher, *European Physical Journal E*, 2003, **12**, 103–107.
- 24 C. B. Roth, A. Pound, S. W. Kamp, C. A. Murray and J. R. Dutcher, *European Physical Journal E*, 2006, **20**, 441–448.
- 25 K. Paeng and M. D. Ediger, *Macromolecules*, 2011, **44**, 7034–7042.
- 26 R. D. Priestley, M. K. Mundra, N. J. Barnett, L. J. Broadbelt and J. M. Torkelson, *Australian Journal of Chemistry*, 2007, **60**, 765–771.
- 27 M. K. Mundra, S. K. Donthu, V. P. Dravid and J. M. Torkelson, *Nano Letters*, 2007, **7**, 713–718.
- 28 J. E. G. Lipson and S. T. Milner, *European Physical Journal B*, 2009, **72**, 133.
- 29 J. L. Keddie, R. A. L. Jones and R. A. Cory, *Faraday Discussions*, 1994, **98**, 219.
- 30 O. K. C. Tsui and H. F. Zhang, *Macromolecules*, 2001, **34**, 9139–9142.
- 31 M. F. Thees and C. B. Roth, *Journal of Polymer Science Part B: Polymer Physics*, 2019, **57**, 1224–1238.
- 32 R. Seemann, K. Jacobs, K. Landfester and S. Herminghaus, *Journal of Polymer Science Part B: Polymer Physics*, 2006, **44**, 2968–2979.
- 33 S. Herminghaus, K. Jacobs and R. Seemann, *European Physical Journal E*, 2001, **5**, 531–538.
- 34 S. Samanta, G. Huang, G. Gao, Y. Zhang, A. Zhang, S. Wolf, C. N. Woods, Y. Jin, P. J. Walsh and Z. Fakhraai, *Journal of Physical Chemistry B*, 2019, **123**, 4108–4117.
- 35 O. K. C. Tsui, T. P. Russell and C. J. Hawker, *Macromolecules*, 2001, **34**, 5535 – 5539.
- 36 D. Christie, C. Zhang, J. Fu, B. Koel and R. D. Priestley, *Journal of Polymer Science Part B: Polymer Physics*, 2016, **54**, 1776–1783.
- 37 S.-F. Wang, Z. Jiang, S. Narayanan and M. D. Foster, *Macromolecules*, 2012, **45**, 6210 – 6219.
- 38 Q. He, S. Narayanan, D. T. Wu and M. D. Foster, *ACS Macro Letters*, 2016, **5**, 999 – 1003.
- 39 L. Zhang, R. Elupula, S. M. Grayson and J. M. Torkelson, *Macromolecules*, 2016, **49**, 257 – 268.
- 40 E. Glynos, B. Frieberg, H. Oh, M. Liu, D. W. Gidley and P. F. Green, *Physical Review Letters*, 2011, **106**, 128301.
- 41 B. Frieberg, E. Glynos, G. Sakellariou and P. F. Green, *ACS Macro Letters*, 2012, **1**, 636 – 640.
- 42 B. Frieberg, E. Glynos and P. F. Green, *Physical Review Letters*, 2011, **108**, 268304.
- 43 B. R. Frieberg, E. Glynos, M. Stathouraki, G. Sakellariou and P. F. Green, *Macromolecules*, 2017, **50**, 3719 – 3725.
- 44 E. Glynos, K. J. Johnson, B. Frieberg, A. Chremos, S. Narayanan, G. Sakellariou and P. F. Green, *Physical Review Letters*, 2017, **119**, 227801.
- 45 B. Liu, S. Narayanan, D. T. Wu and M. D. Foster, *Macromolecules*, 2013, **46**, 3190 – 3197.
- 46 S.-F. Wang, S. Yang, J. Lee, B. Akgun, D. T. Wu and M. D. Foster, *Physical Review Letters*, 2013, **111**, 068303.
- 47 F. Zhang, Q. He, Y. Zhou, S. Narayanan, C. Wang, B. D. Vogt and M. D. Foster, *ACS Macro Letters*, 2018, 834 – 839.
- 48 J. M. Torres, C. M. Stafford, D. Uhrig and B. D. Vogt, *Journal of Polymer Science Part B: Polymer Physics*, 2012, **50**, 370–377.
- 49 T. B. Karim and G. B. McKenna, *Polymer*, 2013, **54**, 5928 – 5935.
- 50 E. C. Glor and Z. Fakhraai, *Journal of Chemical Physics*, 2014, **141**, 194505.
- 51 T. Lan and J. M. Torkelson, *Polymer*, 2014, **55**, 1249–1258.
- 52 S. Askar, T. Wei, A. W. Tan and J. M. Torkelson, *Journal of Chemical Physics*, 2017, **146**, 203323.
- 53 K. Geng, F. Chen and O. K. C. Tsui, *Journal of Non-Crystalline Solids*, 2015, **407**, 296 – 301.
- 54 K. Geng and O. K. C. Tsui, *Macromolecules*, 2016, **49**, 2671 – 2678.
- 55 Z. Yang, Y. Fujii, F. K. Lee, C.-H. Lam and O. K. C. Tsui, *Science*, 2010, **328**, 1676–1679.
- 56 D. Qi, C. R. Daley, Y. Chai and J. A. Forrest, *Soft Matter*, 2013, **9**, 8958 – 8964.
- 57 Z. Yang, A. Clough, C.-H. Lam and O. K. C. Tsui, *Macromolecules*, 2011, **44**, 8294–8300.
- 58 R. N. Li, F. Chen, C.-H. Lam and O. K. C. Tsui, *Macromolecules*, 2013, **46**, 7889 – 7893.
- 59 F. Chen, D. Peng, C.-H. Lam and O. K. C. Tsui, *Macromolecules*, 2015, **48**, 5034 – 5039.
- 60 W. Zhang and L. Yu, *Macromolecules*, 2016, **49**, 731 – 735.
- 61 J. H. Kim, J. Jang and W.-C. Zin, *Langmuir*, 2000, **16**, 4064–4067.
- 62 C. G. Campbell and B. D. Vogt, *Polymer*, 2007, **48**, 7169–7175.
- 63 J. M. Torres, C. Wang, E. B. Coughlin, J. P. Bishop, R. A. Register, R. A. Riggleman, C. M. Stafford and B. D. Vogt, *Macromolecules*, 2011, **44**, 9040–9045.
- 64 A. Shavit and R. A. Riggleman, *Macromolecules*, 2013, **46**, 5044–5052.
- 65 A. N. Storey, W. Zhang, J. F. Douglas and F. W. Starr, *Macromolecules*, 2020, **53**, 9654–9664.
- 66 R. J. Lang and D. S. Simmons, *Macromolecules*, 2013, **46**, 9818–9825.
- 67 P. Z. Hanakata, J. F. Douglas and F. W. Starr, *Nature Communications*, 2014, **5**, 4163.
- 68 C. M. Evans, H. Deng, W. F. Jager and J. M. Torkelson, *Macromolecules*, 2013, **46**, 6091–6103.
- 69 J. H. Mangalara, M. D. Marvin, N. R. Wiener, M. E. Mackura and D. S. Simmons, *Journal of Chemical Physics*, 2017, **146**, 104902.
- 70 J. E. Pye, K. A. Rohald, E. A. Baker and C. B. Roth, *Macromolecules*, 2010, **43**, 8296 – 8303.
- 71 R. D. Priestley, L. J. Broadbelt and J. M. Torkelson, *Macro-*

- molecules*, 2005, **38**, 654–657.
- 72 Y. P. Koh and S. L. Simon, *Journal of Polymer Science Part B: Polymer Physics*, 2008, **46**, 2741–2753.
- 73 Y. P. Koh and S. L. Simon, *Journal of Chemical Physics*, 2017, **146**, 203329.
- 74 R. D. Priestley, C. J. Ellison, L. J. Broadbelt and J. M. Torkelson, *Science*, 2005, **309**, 456–459.
- 75 R. P. White and J. E. G. Lipson, *Physical Review E*, 2011, **84**, 041801.
- 76 R. P. White, C. C. Price and J. E. G. Lipson, *Macromolecules*, 2015, **48**, 4132 – 4141.
- 77 W. E. Wallace, N. C. Beck Tan, W. L. Wu and S. Satija, *Journal of Chemical Physics*, 1998, **108**, 3798–3804.
- 78 J. A. Forrest, K. Dalnoki-Veress and J. R. Dutcher, *Physical Review E*, 1998, **58**, 6109.
- 79 S. Ata, K. Kuboyama, K. Ito, Y. Kobayashi and T. Ougizawa, *Polymer*, 2012, **53**, 1028–1033.
- 80 G. Vignaud, M. S. Chebil, J. K. Bal, N. Delorme, T. Beuvier, Y. Grohens and A. Gibaud, *Langmuir*, 2014, **30**, 11599–11608.
- 81 A. B. Unni, G. Vignaud, J. P. Chapel, J. Giermanska, J. K. Bal, N. Delorme, T. Beuvier, S. Thomas, Y. Grohens and A. Gibaud, *Macromolecules*, 2017, **50**, 1027–1036.
- 82 Y. Han, X. Huang, A. C. W. Rohrbach and C. B. Roth, *Journal of Chemical Physics*, 2020, **153**, 044902.
- 83 X. Huang and C. B. Roth, *Journal of Chemical Physics*, 2016, **144**, 234903.
- 84 B. D. Vogt, *Journal of Polymer Science Part B: Polymer Physics*, 2018, **56**, 9–30.
- 85 C. M. Stafford, B. D. Vogt, C. Harrison, D. Julthongpiput and R. Huang, *Macromolecules*, 2006, **39**, 5095 – 5099.
- 86 J. M. Torres, C. M. Stafford and B. D. Vogt, *ACS Nano*, 2009, **3**, 2677 – 2685.
- 87 J. M. Torres, C. M. Stafford and B. D. Vogt, *Polymer*, 2010, **51**, 4211 – 4217.
- 88 Y. Liu, Y.-C. Chen, S. Hutchens, J. Lawrence, T. Emrick and A. J. Crosby, *Macromolecules*, 2015, **48**, 6534–6540.
- 89 P. A. O’Connell and G. B. McKenna, *Science*, 2005, **307**, 1760–1763.
- 90 P. A. O’Connell and G. B. McKenna, *European Physical Journal E*, 2006, **20**, 143–150.
- 91 P. A. O’Connell, J. Wang, T. A. Ishola and G. B. McKenna, *Macromolecules*, 2012, **45**, 2453–2459.
- 92 S. Xu, P. A. O’Connell and G. B. McKenna, *Journal of Chemical Physics*, 2010, **132**, 184902.
- 93 X. Li and G. B. McKenna, *Macromolecules*, 2015, **48**, 6329–6336.
- 94 H. Yoon and G. B. McKenna, *Macromolecules*, 2017, **50**, 9821–9830.
- 95 S. Mirigian and K. S. Schweizer, *Journal of Chemical Physics*, 2017, **146**, 203301.
- 96 T. B. Karim and G. B. McKenna, *Macromolecules*, 2012, **45**, 9697 – 9706.
- 97 K. Paeng, S. F. Swallen and M. D. Ediger, *Journal of the American Chemical Society*, 2011, **133**, 8444–8447.
- 98 K. Paeng, R. Richert and M. D. Ediger, *Soft Matter*, 2012, **8**, 819 – 826.
- 99 W. Zhang, F. W. Starr and J. F. Douglas, *Journal of Chemical Physics*, 2020, **152**, 124703.
- 100 Z. Fakhraai and J. A. Forrest, *Physical Review Letters*, 2005, **95**, 025701.
- 101 D. D. Vela, A. Ghanekarade and D. S. Simmons, *Macromolecules*, 2020, **53**, 4158–4171.
- 102 C. R. Daley, Z. Fakhraai, M. D. Ediger and J. A. Forrest, *Soft Matter*, 2012, **8**, 2206–2212.
- 103 W. Zhang and L. Yu, *Macromolecules*, 2016, **49**, 731–735.
- 104 L. Zhu, C. W. Brian, S. F. Swallen, P. T. Straus, M. D. Ediger and L. Yu, *Physical Review Letters*, 2011, **106**, 256103.
- 105 Y. Li, W. Zhang, C. Bishop, C. Huang, M. D. Ediger and L. Yu, *Soft Matter*, 2020, **16**, 5062–5070.
- 106 J. A. Forrest and K. Dalnoki-Veress, *ACS Macro Letters*, 2014, **3**, 310 – 314.
- 107 J. D. Stevenson and P. G. Wolynes, *Journal of Chemical Physics*, 2008, **129**, 234514.
- 108 S. F. Swallen, K. L. Kearns, M. K. Mapes, Y. S. Kim, R. J. McMahan, M. D. Ediger, T. Wu, L. Yu and S. Satija, *Science*, 2007, **315**, 353 – 356.
- 109 M. D. Ediger, *Journal of Chemical Physics*, 2017, **147**, 210901.
- 110 S. S. Dalal and M. D. Ediger, *Journal of Physical Chemistry Letters*, 2012, **3**, 1229–1233.
- 111 C. Swanberg, *Macromolecules*, 2007, **40**, 312 – 315.
- 112 H. Bodiguel and C. Fretigny, *Macromolecules*, 2007, **40**, 7291 – 7298.
- 113 J. Wang and G. B. McKenna, *Macromolecules*, 2013, **46**, 2485–2495.
- 114 J. Wang and G. B. McKenna, *Journal of Polymer Science Part B: Polymer Physics*, 2013, **51**, 1343–1349.
- 115 D. Qi, Z. Fakhraai and J. A. Forrest, *Physical Review Letters*, 2008, **101**, 096101.
- 116 J. S. Sharp and J. A. Forrest, *Physical Review E*, 2003, **67**, 031805.
- 117 R. R. Baglay and C. B. Roth, *Journal of Chemical Physics*, 2017, **146**, 203307.
- 118 R. A. L. Jones and R. W. Richards, *Polymers at Surfaces and Interfaces*, Cambridge University Press, Cambridge, UK, 1999.
- 119 C. B. Roth, K. L. McNerny, W. F. Jager and J. M. Torkelson, *Macromolecules*, 2007, **40**, 2568–2574.
- 120 C. B. Roth and J. M. Torkelson, *Macromolecules*, 2007, **40**, 3328–3336.
- 121 C. M. Evans, S. Kim, C. B. Roth, R. D. Priestley, L. J. Broadbelt and J. M. Torkelson, *Polymer*, 2015, **80**, 180 – 187.
- 122 H. Yoon and G. B. McKenna, *Macromolecules*, 2014, **47**, 8808–8818.
- 123 P. M. Rauscher, J. E. Pye, R. R. Baglay and C. B. Roth, *Macromolecules*, 2013, **46**, 9806 – 9817.

- 124 R. Y. F. Liu, Y. Jin, A. Hiltner and E. Baer, *Macromolecular Rapid Communications*, 2003, **24**, 943–948.
- 125 R. Y. F. Liu, T. E. Bernal-Lara, A. Hiltner and E. Baer, *Macromolecules*, 2005, **38**, 4819–4827.
- 126 K. Arabeche, L. Delbreilh, R. Adhikari, G. H. Michler, A. Hiltner, E. Baer and J.-M. Saiter, *Polymer*, 2012, **53**, 1355–1361.
- 127 R. J. Lang, W. L. Merling and D. S. Simmons, *ACS Macro Letters*, 2014, **3**, 758 – 762.
- 128 N. B. Tito, J. E. G. Lipson and S. T. Milner, *Soft Matter*, 2013, **9**, 9403 – 9413.
- 129 R. R. Baglay and C. B. Roth, *Journal of Chemical Physics*, 2015, **143**, 111101.
- 130 D. F. Siqueira, D. W. Schubert, V. Erb, M. Stamm and J. P. Amato, *Colloid and Polymer Science*, 1995, **273**, 1041–1048.
- 131 A. Karim, A. Mansour, G. P. Felcher and T. P. Russell, *Physical Review B*, 1990, **42**, 6846–6849.
- 132 M. Stamm, S. Hüttenbach, G. Reiter and T. Springer, *Europhysics Letters*, 1991, **14**, 451–456.
- 133 T. P. Lodge and T. C. B. McLeish, *Macromolecules*, 2000, **33**, 5278–5284.
- 134 S. K. Kumar, S. Shenogin and R. H. Colby, *Macromolecules*, 2007, **40**, 5759–5766.
- 135 Y. He, T. R. Lutz and M. D. Ediger, *Journal of Chemical Physics*, 2003, **119**, 9956–9965.
- 136 B. L. Kasavan, R. R. Baglay and C. B. Roth, *Macromolecular Chemistry and Physics*, 2018, **219**, 1700328.
- 137 Y. J. Gagnon and C. B. Roth, *ACS Macro Letters*, 2020, **9**, 1625–1631.
- 138 J. A. Forrest and K. Dalnoki-Veress, *Journal of Polymer Science Part B: Polymer Physics*, 2001, **39**, 2664 – 2670.
- 139 H.-J. Butt, K. Graft and M. Kappl, *Physics and Chemistry of Interfaces*, Wiley-VCH Verlag GmbH, Weinheim, Germany, 3rd edn, 2013.
- 140 C. B. Roth and R. R. Baglay, *Polymer Glasses*, CRC Press, Boca Raton, FL, 2016, ch. 1: Fundamentals of Polymers and Glasses, pp. 3 – 22.
- 141 A. Falsafi, S. Mangipudi and M. J. Owen, *Physical Properties of Polymers Handbook*, Springer, New York, 2007, ch. Surface and Interfacial Properties, pp. 1011–1020.
- 142 J. S. Rowlinson and B. Widom, *Molecular Theory of Capillarity*, Clarendon Press, Oxford, 1982.
- 143 K. Binder, J. Baschnagel and W. Paul, *Progress in Polymer Science*, 2003, **28**, 115 – 172.
- 144 P. Scheidler, W. Kob and K. Binder, *Europhysics Letters*, 2002, **59**, 701 – 707.
- 145 P. Scheidler, W. Kob and K. Binder, *Journal of Physical Chemistry B*, 2004, **108**, 6673 – 6686.
- 146 P. Z. Hanakata, B. A. P. Betancourt, J. F. Douglas and F. W. Starr, *Journal of Chemical Physics*, 2015, **142**, 234907.
- 147 G. D. Smith, D. Bedrov and O. Borodin, *Physical Review Letters*, 2003, **90**, 226103.
- 148 T. Davris and A. V. Lyulin, *Journal of Chemical Physics*, 2015, **143**, 074906.
- 149 X. Huang, M. F. Thees, W. B. Size and C. B. Roth, *Journal of Chemical Physics*, 2020, **152**, 244901.
- 150 C. Cao, X. Huang, C. B. Roth and E. R. Weeks, *Journal of Chemical Physics*, 2017, **147**, 224505.
- 151 A. Panagopoulou, C. Rodríguez-Tinoco, R. P. White, J. E. G. Lipson and S. Napolitano, *Physical Review Letters*, 2020, **124**, 027802.
- 152 A. Beena Unni, K. Chat, D. M. Duarte, M. Wojtyniak, M. Geppert-Rybczyńska, J. Kubacki, R. Wrzalik, R. Richert and K. Adrjanowicz, *Polymer*, 2020, **199**, 122501.
- 153 X. Huang and C. B. Roth, *ACS Macro Letters*, 2018, **7**, 269 – 274.
- 154 C. Clarke, *Polymer*, 1996, **37**, 4747–4752.
- 155 K. P. O'Connor and T. C. B. McLeish, *Macromolecules*, 1993, **26**, 7322–7325.
- 156 R. R. Baglay and C. B. Roth, *ACS Macro Letters*, 2017, **6**, 887 – 891.
- 157 A. D. Phan and K. S. Schweizer, *Journal of Chemical Physics*, 2019, **150**, 044508.
- 158 A. D. Phan and K. S. Schweizer, *Macromolecules*, 2019, **52**, 5192–5206.
- 159 D. Diaz-Vela, J.-H. Hung and D. S. Simmons, *ACS Macro Letters*, 2018, **7**, 1295–1301.
- 160 C. M. Evans and J. M. Torkelson, *Macromolecules*, 2012, **45**, 8319–8327.
- 161 D. Christie, R. A. Register and R. D. Priestley, *ACS Central Science*, 2018, **4**, 504–511.
- 162 D. Christie, R. A. Register and R. D. Priestley, *Physical Review Letters*, 2018, **121**, 247801.
- 163 U. Gaur and B. Wunderlich, *Macromolecules*, 1980, **13**, 1618–1625.
- 164 C. G. Robertson, T. E. Hogan, M. Rackaitis, J. E. Puskas and X. Wang, *Journal of Chemical Physics*, 2010, **132**, 104904.
- 165 M. P. Allen and D. J. Tildesley, *Computer Simulation of Liquids*, Oxford University Press, Oxford, UK, 2nd edn, 2017.

## Biography

Connie B. Roth is a Professor of Physics at Emory University with PhD and MSc Physics degrees from University of Guelph, and postdocs at Simon Frazier University and Northwestern University. Her BSc Physics is from McMaster University, while working summers at Xerox Research Center of Canada. Dr. Roth has received NSF CAREER, ACS PRF Doctoral New Investigator, and 2009 Division of Polymer Physics (DPOLY)/UKPPG Polymer Lecture Exchange awards. In 2019, she was named American Physical Society (APS) Fellow and received the Fellows Award from North American Thermal Analysis Society, serving as 2020 DPOLY Program Chair for APS March Meeting.

